Chapter 3
Nanoscale Photovoltaics and the Terawatt Challenge

Stephen M. Goodnick, Nikolai Faleev, and Christiana Honsberg

Abstract Achieving a sustainable energy system providing terawatts (TWs) of electricity is one of the defining challenges of the coming decades. Photovoltaic technology provides the most likely path to realizing TW scale conversion of solar energy in the future and has been on a nearly 40% growth curve over the past two decades. In order to maintain this rapid level of growth, innovations in cell design and conversion efficiency are needed that are compatible with existing technology and can lead to improved performance and lower cost. Nanotechnology offers a number of advantages to realizing such innovation, by providing new materials and the implementation of advanced concepts that circumvent the current physical limits on efficiency. This chapter reviews several of the promising applications of nanotechnology to photovoltaic technologies and their prospects for the future.

3.1 Terawatt Challenge in Photovoltaics

3.1.1 Introduction to Photovoltaics

Achieving a sustainable energy system is one of the defining challenges of the coming decades. The importance and difficulty of developing an energy source which can replace the existing electrical infrastructure is often termed the "Terawatt Challenge," referring to the fact that to supply the energy demands of the globe, truly massive amounts of electricity—terawatts (TW)—are needed [1, 2]. Since the term received broad public airing in 2005, addressing the TW challenge has been given additional impetus and become time critical due to a convergence of multiple issues, including global warming; the scarcity, uneven geographical

S.M. Goodnick (✉) • N. Faleev • C. Honsberg
School of Electrical, Computer and Energy Engineering, Arizona State University,
P.O. Box 875706, Tempe, AZ 85287-5706, USA
e-mail: stephen.goodnick@asu.edu

A. Korkin and D.J. Lockwood (eds.), *Nanoscale Applications for Information and Energy Systems*, Nanostructure Science and Technology,
DOI 10.1007/978-1-4614-5016-0_3,

distribution and cost of conventional resources, particularly oil[1]; and other factors such as aging existing infrastructure, the desirability of local electricity production, or the creation of jobs. At the same time as meeting the TW challenge has become more important, the continuing rapid expansion of renewable technologies has simultaneously offered a solution to the seemingly intractable problem. In the seven years since the term was coined, the installed photovoltaic capacity has quadrupled, and Germany, Spain, and Japan's yearly PV installations meet these countries' annual increase in electricity demand. Yet even in these countries, the overall fraction of the electricity demand met by PV is only a few percent. In order for PV to make a larger contribution, both in the US and worldwide, it must continue its rapid growth and expansion.

Photovoltaic energy conversion is the newest of the energy conversion mechanisms which are suggested for large-scale electricity generation. While the effect was first recorded in 1848 by Bequerel with selenium diodes, its understanding and development depended on the theoretical underpinnings provided by quantum mechanics and solid state theory, as well as on the enormous growth and infrastructure associated with the semiconductor industry. The first practical solar cell was demonstrated in 1954 at Bell Laboratories. Impressively, the first module was installed a few years later in Georgia. Perhaps even more so than the transistor, the first solar cells must have seemed astonishing—batteries at the time were relatively large, so something so small that could power a radio was truly an innovation.

Since that time, the transistor and many other semiconductor devices have traced a trajectory of explosive growth and impact, dramatically improving performance, even exceeding assumed fundamental performance limits. Today, photovoltaics has seen the beginning of similarly explosive growth, and since the mid-2000s has used more silicon than the semiconductor industry. As illustrated in Fig. 3.1, the learning curve for photovoltaic modules, along with that for balance of system (BOS) components (the costs not directly associated with the cell and module itself) shows a rapid, constant learning rate over six orders of magnitude of cumulative production. Despite this fact, photovoltaics is just at the beginning of further growth, and to impact on the overall energy picture, it must grow by another two orders of magnitude. Importantly, as shown in Fig. 3.1, if photovoltaics maintains its historical growth rates, within a decade it will make large and substantial contributions to electricity generation, with yearly world electricity generation equal to the US total electricity demand and with the new installation installed from then on exceeding the yearly increases in world electricity demand.

Despite the impressive growth and increasing impact of photovoltaics, as well as the continually increasing efficiency, the performance of photovoltaics still lags far behind that predicted by thermodynamics. In contrast to both a semiconductor device technology or an electrical generating technology, photovoltaics has

[1] Oil is not used for large-scale electricity production, but is coupled through suggestions of shifting transport demand to either natural gas derivatives (which impacts peaking power for electricity) or directly though electric hybrids.

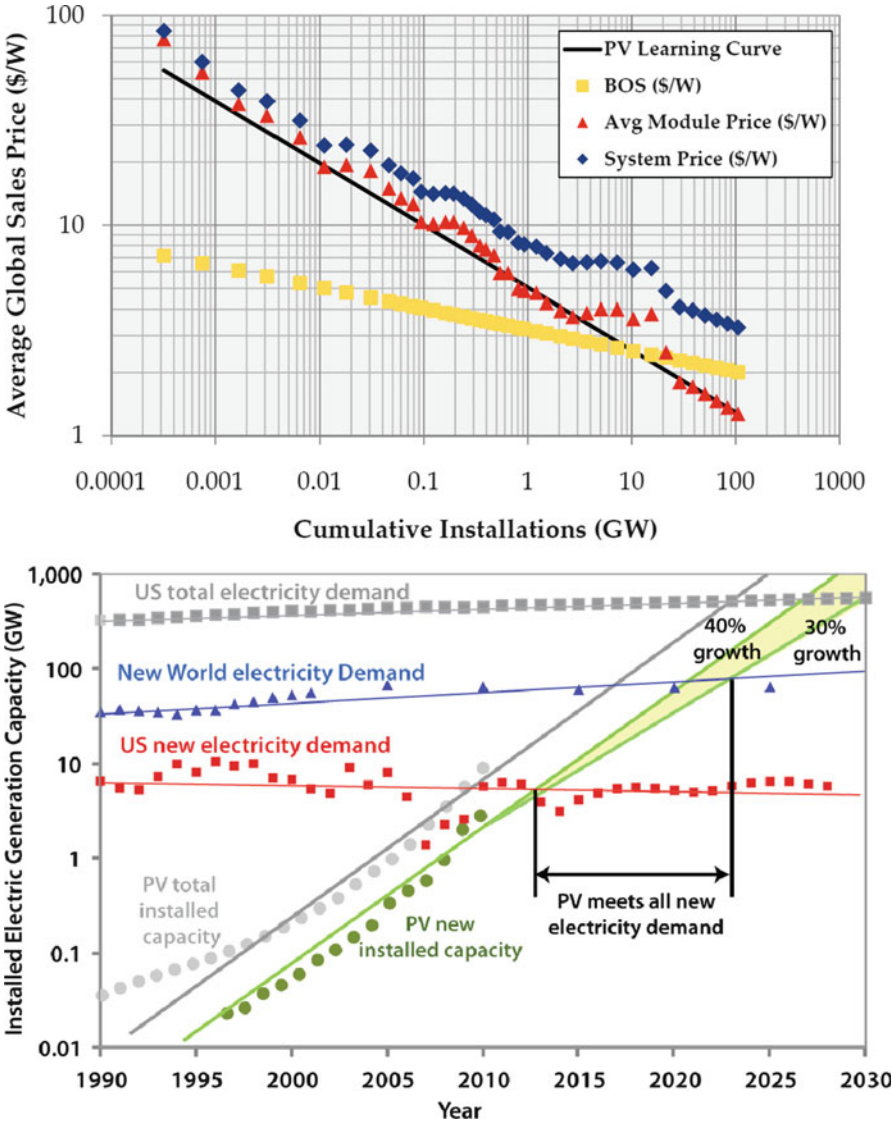

Fig. 3.1 Photovoltaic cumulative production and annually added photovoltaics capacity compared to new US and world electricity demand and the total US electricity demand. The two curves for new installed PV capacity represent continued growth and 40 % compound annual growth rate (CAGR) and 30 % CAGR

achieved less than half of its thermodynamic maximum. On an individual material basis, it does much better, achieving about 75–80% of its material-specific thermodynamic limits, which still leaves substantial room for improvement compared to other devices or electricity systems. Thus, one of the central questions in

photovoltaics is why have efficiencies not reached similar levels of optimization as in other technologies. At first, this may seem like an important problem only for researchers. However, both the experience curve and the costing equations for photovoltaics show that achieving high efficiency at low cost is a critical goal for photovoltaics. The answer to the question of why existing semiconductor approaches have not reached thermodynamics energy conversion limits lies in the fact that the principal technologies of conventional semiconductor devices based on pn junctions and metal oxide semiconductor interfaces are poorly suited to implementing the optimum device structure thermodynamically. New physical mechanisms and material properties enabled by nanotechnology suggest approaches to realizing thermodynamic efficiency limits, but require development and exploitation of effects which are not dominant or even nonexistent in conventional approaches. In the following, we briefly review why efficiency is important for photovoltaics, the thermodynamic efficiency limits and implications for photovoltaics, and how nanostructures can improve existing devices and allow devices near the thermodynamic maximum.

A simple equation for the cost of electricity (COE) in \$/kWh for photovoltaics is given by:

$$\mathrm{COE} = \frac{(\$/m^2{}_{\mathrm{PV}} + \$/m^2_{\mathrm{BOS}})}{\eta \times S} \times \text{Financing Cost} \tag{3.1}$$

where η is the solar cell efficiency, S is the annual incident solar insolation, \$/m^2 PV is the per area cost of the photovoltaics, and \$/m^2 BOS is the cost of balance of system (BOS) components, which as mentioned earlier includes nonpower producing elements, including land, wiring, and power conditioning. Equation (3.1) shows that as the cost of photovoltaics decreases, the BOS costs become an increasing portion of the overall costs. Since many of the BOS or nonpower producing components (glass, land, wiring, etc.) are less subject to large cost reductions, reducing BOS costs by other approaches becomes important. Increasing the efficiency drives costs down in multiple ways. Efficiency not only directly reduces cost by appearing in the denominator of (3.1), a higher efficiency system will have a lower area, and hence BOS costs (the second term in the numerator) are also decreased. Figure 3.2 plots the above equation, which shows that to achieve low eventual system costs, higher efficiencies are necessary.

3.1.2 Limits of Conversion Efficiency

Photovoltaics, compared to other semiconductor devices, have the unusual advantage that the performance (efficiency) can be calculated independent of material assumptions from thermodynamic considerations. One of the first papers to do so is Shockley and Queisser's 1961 paper [3] based on an idealized description of a solar

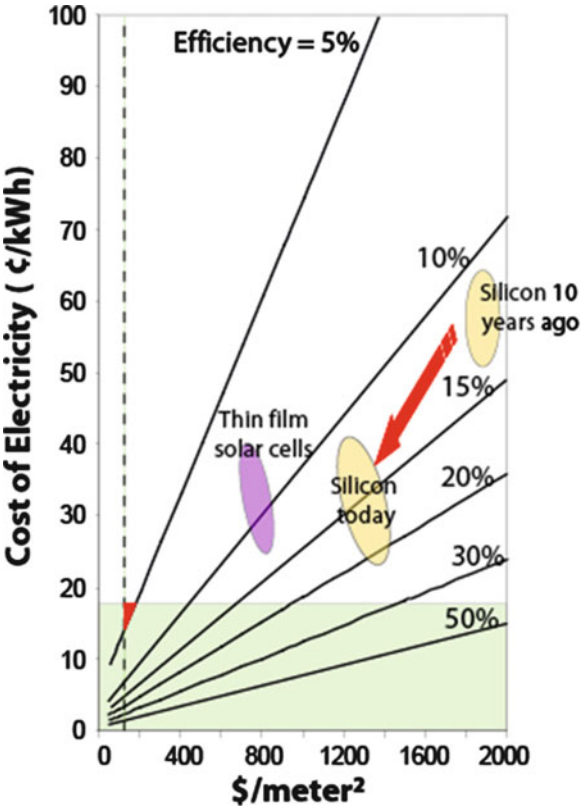

Fig. 3.2 Levelized cost of electricity (LCOE) versus system cost for different conversion efficiencies demonstrating the impact of higher efficiency on the overall cost of electricity

converter which includes no details of the cell structure itself, rather it assumes complete collection of available photogenerated carriers with the following basic assumptions (1) radiative recombination only; (2) one band gap; (3) absorption across the band gap in which one photon generates one electron–hole pair; (4) one associated quasi-Fermi level separation with each band gap; (5) constant temperature in which the carrier temperature is equal to the lattice and ambient temperature; and (6) steady state, which is close to equilibrium. The result of this type of calculation, referred to as *detailed balance*, is illustrated in Fig. 3.3, where the black curve is the calculated efficiency versus bandgap for an AM1.5 solar spectrum (roughly corresponding to terrestrial solar spectrum). The maximum efficiency without concentration is around 33.7% corresponding to maxima around 1.1 and 1.4 eV (the former value being close to the Si bandgap). The principal losses are due to the loss of photons with energy below the bandgap and loss of the excess energy of the photon above the bandgap in terms of energy relaxation of photoexcited carriers back to the band edges. The trade-off between these two loss mechanisms leads to the maximum efficiency as shown in Fig. 3.3.

In their paper, they also examined the effects of nonradiative recombination, and the concept of using multiple bandgaps (tandems) to circumvent the single gap limit

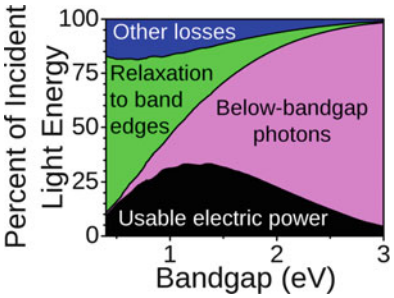

Fig. 3.3 Breakdown of the various loss mechanisms contributing to the single bandgap Shockley–Queisser efficiency limit. The *black shaded region* represents the calculated AM1.5 solar spectrum conversion efficiency as a function of bandgap, while the other *shaded regions* represent the losses (source: Wikipedia Commons)

shown earlier had already been introduced as early as 1955. The next 30 years in photovoltaics focused largely on increasing the efficiency of single and multiple band gap solar cells, and in the mid-1990s silicon had achieved an efficiency of 25% (a "champion result which still stands"). Tandem solar cells also saw efficiency increases, although here the efficiency of champion solar cells is still increasing [4].

During this time, detailed balance and thermodynamic analyses continued to progress, including tandems, photon recycling, and other effects into the analysis. However, with only a small number of exceptions (most notably Nozik and Ross in 1982 [5]), the remainder of the assumptions of Shockley and Queisser were not examined. In 1990, Barnham and Duggan [6] made the suggestion that a quantum well solar cell could achieve the voltage of the larger band gap, but the current of the smaller, and S. Kolodinski et al. measured quantum efficiencies [7]. These papers sparked a re-examination of thermodynamic and detailed balance limits, as well as multiple suggestions of approaches to improve efficiencies above a single junction limit.

Photovoltaics energy conversion is distinct from other electricity generation mechanisms in that it directly converts sunlight into electricity. All other electricity generation mechanisms ultimately rely on a generator, converting mechanical energy into electrical energy. Most of the electricity generation approaches (with the exception of wind and hydropower) are thermodynamically similar in that they convert a heat source into electrical energy. The thermodynamics of such approaches are understood as a heat engine—an energy source heats a reservoir, and energy is extracted from the reservoir. The thermodynamics of most solar cells are a "quantum converter," in which an electron(s) interacts with a photon (or photons). Thermodynamically, photovoltaics is most similar to a Stefan–Boltzmann engine. The energy from the photon must be converted to another state or it is lost—unlike a heat engine where the excess heat may be retained by the thermal reservoir. While the maximum thermodynamic efficiency under maximum concentration and completely optimum assumptions is the same

Table 3.1 Comparison of photothermal and photovoltaic approaches as a function of the number of band gaps and concentration (C)

C	Number of band gaps	Photo-thermal	Photo-voltaic
1	1	53.6	31.0
	2	60.9	42.9
	3	63.3	49.3
	...	...	...
	∞	68.2	68.2
100	1	67.0	35.2
	2	71.7	48.4
	3	73.2	55.6
	...	...	...
	∞	76.2	76.2
46,300	1	85.4	40.8
	2	86.1	55.7
	3	86.3	63.9
	...	...	...
	∞	86.8	86.8

between a quantum converter and a thermal converter, their thermodynamic efficiency under noninfinite concentration or noninfinite number of "band gaps" varies considerably. This fact is presented in Table 3.1, which shows that a thermal converter (e.g. a power plant) is very dependent on concentration (i.e., the operating temperature of the converter). This relationship is well known and understood for thermal power plants, with practical and material limits giving a roughly 30% efficiency for these electricity generating schemes, regardless of whether the heat source is nuclear, coal, or solar thermal. However, unlike the case of power plants, in a solar converter where the carrier temperature drives the thermal engine, the carrier temperature can be substantially elevated under solar concentration, providing increased efficiency, as seen in Table 3.1. In conventional photovoltaic approaches, because they are a quantum converter, the photon energy above the band gap is lost. Concentration makes a small difference in efficiency, largely because the quasi-Fermi levels move closer to the band gap, where the lost energy above the band gap is the largest driving factor, and can only be overcome by using a stack of band gaps (called tandem solar cells). The efficiency as a function of band gap and concentration is shown in Fig. 3.4.

The re-examination of thermodynamics gave rise to the realization that the assumptions 3–6 in the detailed balance examination are not thermodynamically inherent, and that approaches that can overcome these assumptions will give rise to higher efficiencies. A summary of the key approaches that are used to overcome these assumptions is given in Table 3.2. Of these, the ones with the most experimental and theoretical investigation are intermediate band solar cells, multiple exciton solar cells, and hot carrier solar cells. These are discussed in Sect. 3.3.

The above discussion highlights why existing solar cells have not reached their overall thermodynamic efficiency limits, even though they have reached their material-imposed efficiency limits. A p–n junction, even a stack of p–n junctions, is not the thermodynamic ideal—for example, a stack of 8 solar cells or more is

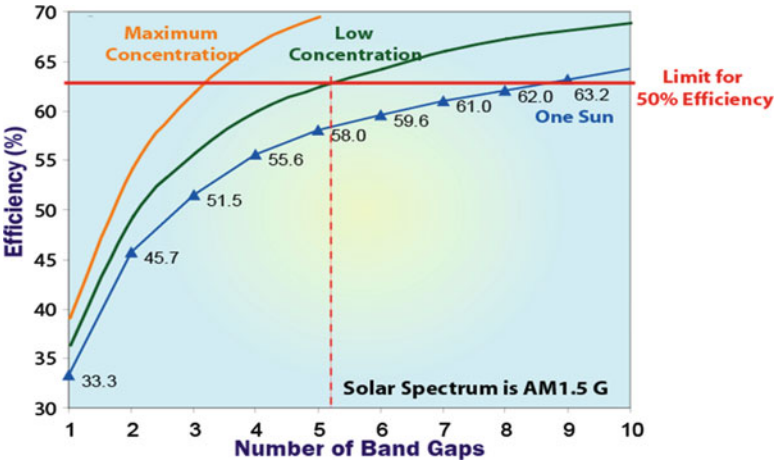

Fig. 3.4 Calculated detailed balance (thermodynamic) efficiency of an ideal solar converter as a function of the number of bandgaps in a tandem cell configuration, for three different concentrations of AM1.5 spectrum sunlight

Table 3.2 Advanced concept solar cell approaches

Assumption in Shockley–Queisser	Approach which circumvents assumption	Examples
Input is solar spectrum	*Multiple spectrum solar cells*: transform the input spectrum to one with same energy but narrower wavelength range	Up/down conversion Thermophotonics
1 photon = 1 electron–hole pair	*Multiple absorption path solar cells*: any absorption path in which one photon ≠ one electron–hole pair	Impact ionization, MEG, two-photon absorption
One quasi-Fermi level separation	*Multiple energy level solar cells*: Existence of multiple meta-stable light-generated carrier populations within a single device	Intermediate band quantum well solar cells
Constant temperature = cell temperature = carrier temperature	*Multiple temperature solar cells*: Any device in which energy is extracted from a difference in carrier or lattice temperatures	Hot carrier solar cells
Steady state (≈ equilibrium)	*AC solar cells*: Rectification of electromagnetic wave	Rectenna solar cells

necessary to realize an efficiency approaching the thermodynamic limit. However, thermodynamics indicates that there are structures or physical mechanisms which reach thermodynamic limits—for example, a quantum/thermal hybrid thermodynamic reaches efficiencies of 68% under one sun—close to the thermodynamic maximum of 70%. While the approach to implementing such structures in not clear with conventional semiconductor materials and approaches, it highlights that new physical mechanisms possible in nanostructured materials are key to realizing ultra-high efficiency solar cells.

3.1.3 Existing Solar Cell Technology

The dominant commercial solar cell technology consists of silicon solar cells, comprising over 80% of the market. The most common silicon solar cell is a front junction, screen printed device, consisting of a diffused junction, a silicon nitride surface passivation, silver screen-printed metal front contacts which are fired through the silicon nitride and aluminum/silver rear contacts. The record silicon solar cell is 25%, and commercial modules typically are 14% for multicrystalline and 17% for monocrystalline, with a few commercial technologies having efficiencies close to the record cell results. Thin film solar cells, mostly CdTe but also CIGS (CuInGaSe2) provide a lower fabrication and lower $/W cost, but with lower efficiency. Overall, the two technologies have similar cost of electricity.

A substantially different technology and approach is to make ultra-high efficiency solar cells by growing multiple solar cells in a single solar cells stack. The high cost of these devices is compensated for by using them in an optical concentrator (where the light intensity is 200× to 400× higher than typical sunlight), such that only very small areas are needed. The optical systems must track the sun, and these large systems are suited primarily for utility scale applications. The central issue in such devices is the availability of materials which are lattice matched or nearly so, and also have ideal band gaps. The lack of materials with 1.0 eV lattice matched to GaAs limits the ability to realize substantial efficiency increases, although metamorphic or dilute nitride (InGaAsN) have demonstrated champion efficiencies.

3.1.4 Advanced Concept Solar Cells

As illustrated in Fig. 3.3, the Shockley–Queisser limit is a consequence of the fact that photons below the bandgap of the absorber are not collected, while each absorbed photon above contributes only the energy of the of electron–hole pair at the bandgap, independent of the photon energy. So-called *third generation photovoltaics* refers to solar cell technology in which advanced concepts usually based on nanotechnology are used to circumvent the single gap limit and help drive cost down through improvement in efficiency [8]. Figure 3.5 shows a slightly different representation of Fig. 3.2, illustrating the expected market for new concept solar cells in terms of the cost of electricity. The advantage of higher efficiency allows for higher module cost, and as mentioned earlier, may lead to significant reductions in the BOS costs as well, reducing the overall cost of electricity.

There are a number of paths to approaching thermodynamic conversion efficiencies (~85%) rather than the single gap Shockley–Queisser limit. Table 3.2 gives a summary of different approaches, which go beyond the assumptions inherent in the single band limit. One of the limitations in efficiency implicit in Fig. 3.3 is the fact that the solar spectrum is a broadband source, which leads to the trade-offs in various energy loss mechanisms and the difficulty in optimizing the performance for

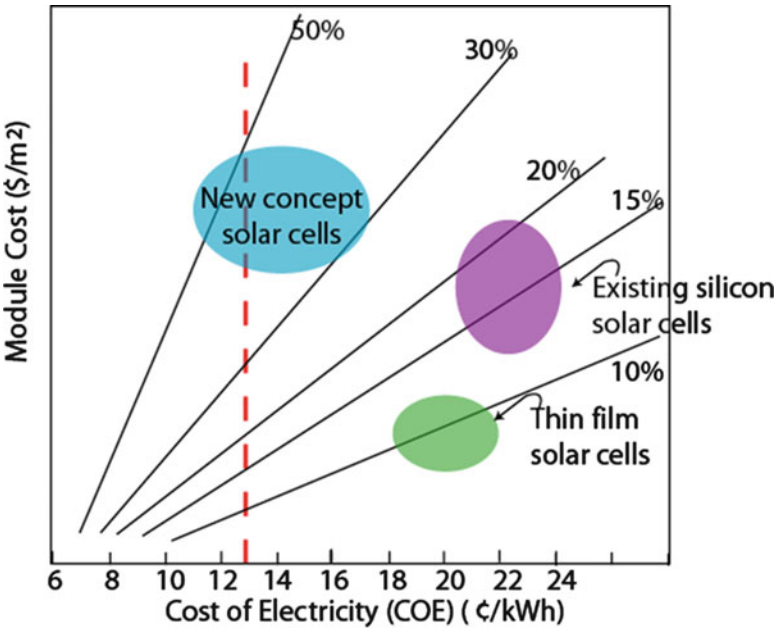

Fig. 3.5 Module cost as a function of levelized cost of electricity (COE) for different conversion efficiencies showing the advantage of high efficiency solar cells in terms of reduced COE

a single gap. If the solar spectrum can be transformed to a narrow spectrum, higher efficiency is possible. Schemes for this include up/down conversion of the solar spectrum through phosphors or two-photon absorption/emission. Conversion of the solar spectrum to thermal energy, and then photovoltaic recapture of the blackbody radiation at a lower temperature (thermophotonics) effectively narrows the solar spectrum as well, and theoretically leads to much higher conversion efficiency.

Another route to exceeding the single gap limit is to generate multiple electron–hole pairs from a single photon through the creation of secondary carriers (band-to-band impact ionization or multiexciton generation) [9]. Particularly promising are nanocrystalline materials, where the reduced dimensionality of the system suppresses competing energy relaxation mechanisms and reduces the threshold for generation of secondary carriers as discussed in Sect. 3.3.2 [10]. The fact that quantum efficiencies greater than unity may be possible, consequently lead to theoretical efficiencies greater than the Shockley–Queisser limit.

Another way to circumvent the single gap limit is to have multiple energy level solar cells. Multijunction or tandem solar cells were already discussed in this context in Sect. 3.1.2 and have shown the highest efficiencies of any solar cell technology [11]. Such cells are grown using epitaxial material growth technology discussed in the next section, which is generally quite expensive compared to conventional Si solar cell production. Hence such cells are targeted for concentrating photovoltaic (CPV) systems, in which high concentration is used to focus sunlight on a small diameter cell area.

An alternate approach to having multiple junctions is to introduce multiple levels within the same material, which provide multiple paths for photon absorption, but collect carriers at the primary bandgap of the host material. Luque and Marti introduced the concept of an intermediate band (IB) solar cell to realize such a structure, and overcome the Shockley–Queisser limit [12], although as mentioned earlier, similar concepts had been suggested for quantum well solar cells. An intermediate level in the bandgap is introduced through, for example, self-assembled quantum dots, which allow low energy photons to excite electron–hole pairs through multiphoton absorption, below the gap of the principal absorber. Such approaches and their implementation with nanostructured systems are discussed in more detail in Sect. 3.3.3.

Finally, one can relax the assumption of constant temperature throughout and allow for nonequilibrium distributions of carriers at different effective energies. Ross and Nozik proposed the concept of hot carrier solar cells [13] 25 years ago as a means to circumvent the limitations imposed by the Shockley–Queisser limit in terms of both the lost of excess kinetic energy and the loss of long wavelength photons. The concept was extended further by Würfel and coworkers considered the effect of impact ionization and secondary carrier generation on the ultimate efficiency of this concept [14, 15]. In this concept, electrons and holes are not collected at the band edges (which limits to the output voltage to the bandgap), rather they are collected through energy selective contacts above and below the conduction and valence band edges, respectively. The absorber material (generally a narrow gap material) suppresses energy loss, so that hot carriers can reach sufficient energy to escape through the energy selective contacts. This concept is discussed later in Sect. 3.3.4.

3.2 Nanostructured Materials and Devices

Nanotechnology, by its name, refers to technology at small scales, literally at nanometer scale dimensions (10^{-9} m). Somewhat arbitrarily, we define nanometer scale to characteristic feature sizes on the order of 100 nm or less in terms of the separation of the micro and nano-worlds. The fact that almost all such structures contain nanoscale features in one form or another has led to "nanotechnology" being regarded as a somewhat broad umbrella encompassing a host of scientific and engineering disciplines.

The nanotechnology "revolution" has been enabled by remarkable advances in atomic scale probes and nanofabrication tools. Structures and images at the atomic scale have been made possible by the invention of the scanning tunneling microscope (STM), and the associated atomic force microscope (AFM), for which Gerd Binning and Heinrich Rohrer from IBM Research Laboratory were awarded the Nobel Prize in 1986 [1]. Such scanning probe microscopy (SPM) techniques allow atomic scale resolution imaging of atomic positions, spectroscopic features, and positioning of atoms on a surface. Top down nanofabrication techniques such as

electron-beam, ion-beam, and deep ultra-violet (UV) lithography allow the patterning of features down to tens of nanometers, and AFM techniques can be used to actually position atoms literally with atomic precision.

Concurrently, there have been significant advances in the "bottom up" synthesis and control of self-assembled materials such as nanoparticles, nanowires, molecular wires, and novel states of carbon such as fullerenes, graphene, carbon nanotubes (CNTs), and composites thereof. These advances have led to an explosion of scientific breakthroughs in studying the unique electronic/optical/mechanical properties of these new classes of materials.

At the same time, such nanostructured materials are emerging as new and improved materials for structural components as well as coatings, insulators, and conductors. Self-assembled materials are also being commercially pursued for potential application as components of electronic devices and circuits. Many energy conversion technologies are also benefiting from the ability to synthesize new nanostructured materials to improve performance or replace costly materials with relatively inexpensive alternatives.

3.2.1 Nanomaterials

Nanomaterials usually refer to materials that have structural features on the nanoscale, and in particular their properties stem from these nanoscale dimensions. Such nanomaterials may include quantum wells, nanoparticles, nanopowders, nanoshells, nanowires, nanorods, nanotubes such as CNTs, nanomembranes and nanocoatings, or combinations of these to form nanocomposites. An important feature of nanomaterials for energy applications compared to their bulk counterparts is that the surface-to-volume ratio is greatly enhanced, resulting in fundamental changes in the chemical, electronic, mechanical, and optical properties, in essence creating a new material. Such changes are a result of the different energies associated with surfaces compared to the bulk. This may result in complete changes in the way materials may behave, in terms of their catalytic properties, their chemical bonding, strength, etc. Another effect is the so-called quantum size effect, which like the simple particle in a box, quantizes the motion of electrons in a solid, meaning the allowed energies can only assume certain discrete values. This generally changes the electrical and optical properties of materials. For example, nanoparticles show a blue shift in their absorption spectrum to high frequency due to quantum confinement effects.

3.2.1.1 Quantum Wells and Superlattices

One of the first truly nanoscale fabrication technologies was the development of precision epitaxial material growth techniques such as molecular beam epitaxy (MBE) [16] and metal organic chemical vapor deposition (MOCVD), through

which high-quality, lattice-matched heterojunction (junction between two dissimilar materials) semiconductor layered systems could be realized, with atomic precision in the interface quality. A sandwich composed of a narrower bandgap material clad with larger bandgap materials of atomic dimensions is referred to as a quantum well (QW), and when many of these are grown sequentially, they are referred to as a multiquantum well (MQW) system. These systems exhibit strong quantum confinement effects due to the low density of defects at the interface of lattice-matched materials such as GaAs and $Al_xGa_{1-x}As$. If the thickness of the barriers separating large and small bandgap materials is reduced so that the electronic states of the QWs overlap, the system is referred to as a superlattice (SL), which behaves as a new material electronically.

The capability of epitaxial growth to realize atomically precise hetero-interfaces has served as the basis for a number of electronic and optoelectronic device technologies including heterojunction bipolar transistors (HBTs), high electron mobility transistors (HEMTs), quantum well lasers, quantum well infrared photodetectors (QWIPs), and quantum cascade lasers (QCLs), to mention a few. In photovoltaic applications, single crystal epitaxial growth is the basis for high efficiency tandem or multijunction solar cells which hold the record for conversion efficiency as discussed earlier. They typically are designed for high performance extraterrestrial applications (spacecraft) or high performance terrestrial concentrating photovoltaic (CPV) applications. MQW systems are also of active interest for QW solar cells or several of the advanced concept devices discussed in the next section.

3.2.1.2 Nanowires

The term *nanowire* generally refers to a high aspect ratio wire-like structures in which the cross-sectional dimensions are nanometer scale, while the length may be micro to macroscale. Nanowires are generally solid, not hollow structures, the latter being referred to as *nanotubes*. Such nanowires may be oxide, metallic, or semiconducting. One of the major broad techniques used for the growth of semiconducting nanowires is *vapor-phase synthesis*, in which nanowires are grown by starting from appropriate gaseous components. In the so-called *vapor–liquid–solid* (VLS) mechanism metallic nanoparticles are used as seed sites to stimulate the self-assembled growth of nanowires. The desired semiconductor system is introduced in terms of its gaseous components and the entire assembly is heated to a temperature beyond the eutectic temperature of the metal/semiconductor system. Under these conditions, the metal forms a liquid droplet, with a typical size of a few nanometers. Once this droplet becomes supersaturated with semiconductor, it essentially nucleates the growth of the nanowire from the base of the droplet. Figure 3.6 shows examples of Si nanowires grown by VLS method using gold nanoparticles as the seeding droplets. The high-crystalline integrity of this nanowire can be clearly seen in this image, which also makes clear how the diameter of the nanowire is connected to the size of the catalyst droplet [17]. The wire shown here was

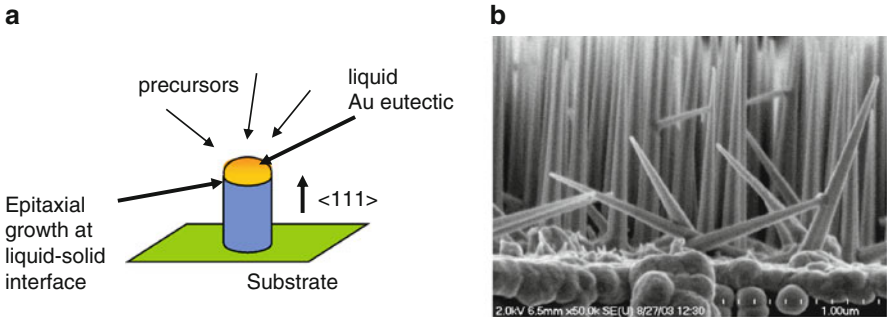

Fig. 3.6 (**a**) Schematic of the self-assembled growth of nanowires using vapor–liquid–solid (VLS) epitaxy. (**b**) Scanning electron microscopic picture of the vertical growth of Si nanowires by VLS epitaxy (from T. Picraux and J. Drucker, unpublished)

grown by using chemical-vapor deposition (CVD) to generate the semiconductor precursors, a popular approach to VLS. Other methods may also be used, however, including laser ablation and MBE. The VLS method has emerged as an extremely popular method for the fabrication of a variety of nanowires. It has also been used to realize various III–V (GaN, GaAs, GaP, InP, InAs) and II–IV (ZnS, ZnSe, CdS, CdSe) semiconductor nanowires, as well as several different wide-bandgap oxides (ZnO, MgO, SiO_2, CdO).

Samuelsson and coworkers have also had enormous success in developing nanoscale electronic devices that utilize VLS-formed, III–V semiconductor, nanowires as their active elements [18]. They have demonstrated that heterostructure nanowires of InAs and InP, as well as GaAs and InAs, can be realized that have very sharp heterointerfaces [19]. They have subsequently used this technique to implement a variety of nanoscale devices, such as resonant-tunneling diodes [20], single- [21], and multiply coupled [22, 23] quantum dots. The strong lateral confinement generated in these structures, combined with their high crystalline quality, endows them with robust quantum-transport characteristics. Quantum dots realized using these structures show very clear single-electron tunneling signatures, with evidence that the g-factor of the electrons can be tuned over a very wide range [24]. The ability to arbitrarily introduce serial heterointerfaces into such nanowires should offer huge potential in the future for the further development of novel nanodevices.

From the perspective of energy conversion, nanowire structures are being researched as new materials for electrochemical storage and energy conversion devices, due to the large volume ratio of these structures, which improves the catalytic performance and reaction rates, as well as providing large internal surface areas for charge storage. Within renewable energy technologies such as solar photovoltaic devices, nanowires are finding increasing use in light management, reducing the amount of light lost and allowing less material to be used for the absorption of light, hence improving efficiency and lowering material cost. Most of these efforts are in the research phase or as part of start-up ventures commercially.

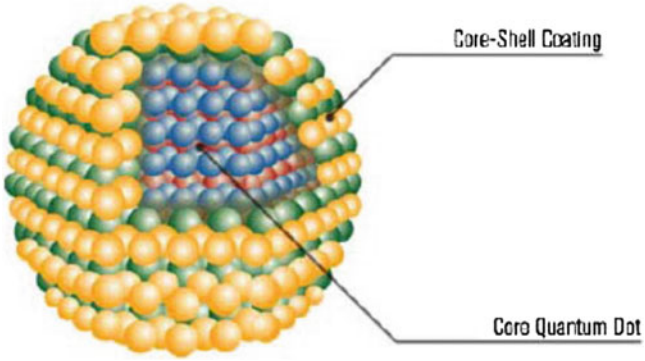

Fig. 3.7 Schematic of a core–shell nanoparticle, nanocrystal, or quantum dot structure with two different compositions

3.2.1.3 Nanoparticles and Quantum Dots

Nanoparticle is a name generally given to ultrafine size particles with dimensions on the order of 1–100 nm. If the nanoparticles are single crystal individual particles, they are often referred to as nanocrystals [25]. Alternately, agglomerates of nanoparticles are referred to as nanopowders. Nanoparticles can be metals, dielectrics, or semiconductors. They can also be grown with different compositions to form core–shell nanoparticles with unique electrical and optical properties, as illustrated in Fig. 3.7. Their electronic and optical properties are different from bulk materials as mentioned before due to quantum size effects which shift the fundamental gap to higher energy. Surface effects also play a dominant role. In particular, the dielectric properties can also be modified by surface plasma resonance effects, which change the absorption properties. The high surface-to-volume ratio affects other properties such as diffusion properties in liquid and the adhesive properties.

Nanoparticles are synthesized by a variety of techniques. One inexpensive method is through ball mill micro-machining to literally grind materials down into nanoparticles. Pyrolysis and rf plasma techniques may also be used. A popular method for synthesizing nanoparticles of high quality is through chemical solution methods, in particular sol-gel methods can realize colloidal solutions of nanoparticles which may be subsequently dried for individual nanoparticles, or the gel solutions cast for particular applications. Another method of realizing semiconductor nanoparticles is through self-assembly of InAs, or InGaAs quantum dots that on a GaAs substrate via the Stransky–Krastinov growth process [26]. In this mode of growth, a thin layer of InAs is grown on top of a GaAs substrate, but, if the layer is sufficiently thin, the strain will cause the InAs to agglomerate into small three-dimensional quantum dots.

Nanoparticles (and other nanomaterials such as nanowires and nanotubes) can be embedded in a host matrix to form a *nanocomposite*. The main differentiating factor between a nanocomposite and a normal composite material is that the large

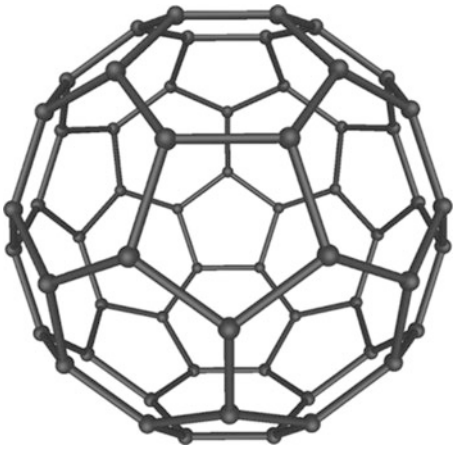

Fig. 3.8 Structure of C_{60}, Buckminsterfullerene

surface-to-volume ratio of the nanoparticle, which means that there is a large internal surface area associated with the nanoparticles compared to normal composite materials. Therefore, a much smaller amount of nanoparticle composition can have a much greater effect on the overall nanocomposite properties. Nanocomposites can be comprised of many forms, the primary ones be ceramic matrix, metal matrix, or polymer matrix nanocomposites.

3.2.1.4 Carbon-Based Materials

One of the major nanomaterials that has led to an explosion in growth in nanotechnology are those based on closed structures of graphene sheets (1 layer of graphite) composed of sp^2 bonded hexagonal rings. The term *fullerene* is used to denote any hollow closed structure such as C_{60} (Buckyballs) and CNTs. Even the properties of graphene itself have become a major focus of research due to their extraordinary electrical and thermal properties. Below we briefly review a few of the major carbon-based technologies. The first fullerene that was discovered was C_{60}, a soccer-ball-shaped object first reported by the Rice University group [27] (who were later awarded the 1996 Nobel Prize in Chemistry), the so named Buckminsterfullerene, shown in Fig. 3.8. Other such fullerenes with 72, 76, 84, etc. carbon atoms have since been synthesized. The most common method of producing C_{60} is through a carbon arc plasma between two graphite electrodes in an inert ambient. C_{60} has also found application in organic electronics and energy applications, and there it can facilitate charge transfer across interfaces. Relative to photovoltaics, they are a common component of organic photovoltaic (OPV) devices as an acceptor material or for improved charge transport.

Single-walled carbon nanotubes (SWCNTs) are a tubular form of carbon with diameters as small as 1 nm and lengths of a few nm to microns. CNTs have received considerable attention due to the ability to synthesize NTs with metallic,

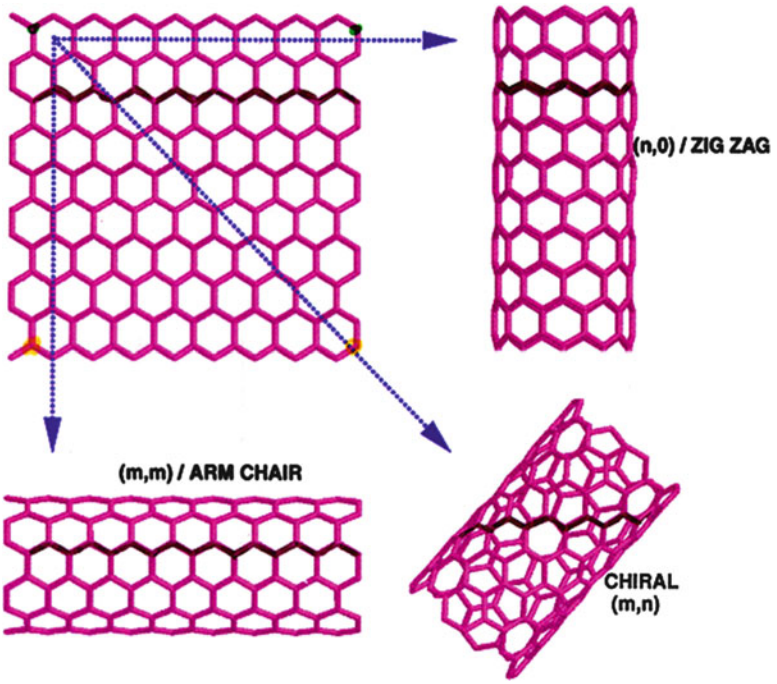

Fig. 3.9 Formation of different chirality CNTs formed by rolling a graphene sheet into a tube

semiconducting, and insulating behavior, depending on the diameter, and particularly on the chirality (i.e., how the graphite sheets forming the structure of the CNT wrap around and join themselves) [28]. Due to their remarkable electronic and mechanical properties, CNTs are currently of interest for number a of applications including interconnects; CNT-based molecular electronics; AFM-based imaging; nanomanipulation; nanotube sensors for force, pressure, and chemical; nanotube biosensors; molecular motors; nanoelectromehanical systems (NEMS); hydrogen and lithium storage; components in solar cells; and field emitters for instrumentation including flat panel displays including optically transparent films.

The structure of a SWCNT is illustrated in Fig. 3.9. It starts with a single monolayer of graphite (graphene), which has a hexagonal lattice structure characteristic of hybridized sp^2 C–C bonding. The graphene sheet may be rolled to join itself in many different ways, characterized by a pair of integers m and n, which signify the number of unit cells in the x and y direction in which the sheet is joined to itself. The larger m and n, the larger the diameter of the nanotube, with a diameter $d = a/\pi\sqrt{n^2 + nm + m^2}$, where $a = 0.246$ nm is the lattice constant. CNTs have very large aspect ratios; while the diameter may be nanometers in dimension, the length may be micron to centimeter scale in length. The ratio of m and n determines the chirality of the CNT, which determines whether it is metallic or

semiconducting. *Zigzag* CNTs correspond to any combination 0, *n*. Another common CNT configuration is the *armchair* CNT corresponding to $n = m$. Generally speaking, armchair CNTs are metallic, with zero bandgap. Zigzag CNTs are semiconducting, unless *n* is a multiple of 3, with a bandgap approximately equal to $0.8/d$ eV, where *d* is the diameter of the nanotube in nanometers.

In addition to SWCNTs, multiwalled carbon nanotubes (MWCNTs) consist of multiple rolled layers (concentric tubes) of graphene. A triple walled, armchair honeycomb carbon nanotube may, for example, be made from three single-walled nanotubes. Another possible arrangement for a multiwall nanotube is by rolling a single sheet of graphene around itself, similar in shape to a snail shell. The distance between the layers is approximately 3.4 Å, which corresponds to the distance between graphene layers in bulk graphite.

In terms of their electronic transport properties, measurements on CNTs have demonstrated very high conductivities, due to the high sheet carrier density in a small dimension, the high carrier mobilities, and nearly ballistic transport [29, 30]. For this reason CNTs have been considered as viable candidates for high performance conductors and interconnects, with higher potential conductivity than copper. In terms of electronics applications, complementary n and p-channel transistors have been fabricated from CNTs, and basic logic functions demonstrated [31]. The primary difficulty faced today in a manufacturable integrated circuit (IC) technology is the directed growth and placement of CNTs with the desired chirality and diameter, suitable for large-scale production.

Typical synthesis methods include the arc discharge of graphite (the original method used to first realize CNTs), pyrolysis/thermal decomposition of a carbon source such as hydrocarbons, or laser ablation. For commercial production, the most common approach however is the catalytic growth of CNTs using chemical vapor deposition (CVD) growth, where typically metal particles are used as a catalyst. As grown, CNTs can be bundled and must be dispersed and separated to access individual nanotubes. In certain processes, like Plasma Enhanced CVD (PECVD), SWCNTs and MWCNTs grow in dense vertical arrays, with diameters and density determined by the size and distribution of the nanoparticle metal catalyst. As a result of their multifunctional properties, CNT polymer composites are expected to be used as low weight structural materials, optical devices, thermal interface materials, electric components, and electromagnetic absorption materials.

3.3 Nanotechnology and Photovoltaics

Nanostructures in solar cells have multiple approaches by which they can improve photovoltaic performance (1) new physical approaches in order to reach thermodynamic limits; (2) allow solar cells to more closely approximate their material-dependent thermodynamic limits; and (3) provide new routes for low-cost fabrication

by self-assembly or design of new materials. Some of the specific advantages and disadvantages presented by nanotechnology are listed as follows:

- Range of bulk materials with proper energy gaps, catalytic properties, etc., is very limited
- Nanostructured materials allow "bandgap engineering" of electronic states and energy gaps: artificial materials
- Provide intermediate energy centers within host material
- Optical absorption can be increased, reflection and other optical losses decreased
- Improve transport and reduce scattering and energy loss
- However, higher surface-to-volume ratio means surface effects dominate: higher recombination

3.3.1 Nanostructures in Existing Solar Cell Technologies

In order to approach the ultimate efficiency limits of 70% at one sun and 86.6% at maximum concentration, new physical mechanisms are necessary. However, there is still enormous room for scope in improving existing devices. Such approaches can in general be classed in two categories: the first uses nanostructures to alter the material properties (primarily band gap) such that a more ideal structure results. For example, in tandem solar cells, the lack of a 1 eV material limits the ability to achieve tandems with a larger number of solar cells in the stack and also reduces the efficiency of existing three-junction solar cells. The use of QDs or QWs can synthesize a region of lower band gap, thus improving efficiency. In order to realize high efficiency, strain compensation for the QW/QD layer is essential. These approaches have been demonstrated in several materials, including GaAs/InAs-based materials, GaAsP-based materials, and dilute nitrides.

A more radical re-design of material properties is to use nanostructures to modify a single band gap material (e.g. Si), allowing a tandem solar cell in a single material. For example, Si can serve as the basis of a tandem solar cell by using QDs with increased band gap to form the upper junctions. Such an approach is illustrated in Fig. 3.10.

3.3.2 Multiexciton

The generation of multiple electron–hole pairs from an absorbed high energy photon provides a mechanism for increasing the efficiency of a single junction solar cell above the Shockley–Queisser limit of 33% under AM1.5 conditions, as shown conceptually in Fig. 3.11. Generation of multiple electron–hole pairs has been known in bulk materials since the 1960s in Ge and has been experimentally demonstrated in bulk silicon solar cells [32]. However, impact ionization or Auger generation processes have a low efficiency in bulk materials, and too high a threshold energy for effective utilization of the solar spectrum due to crystal

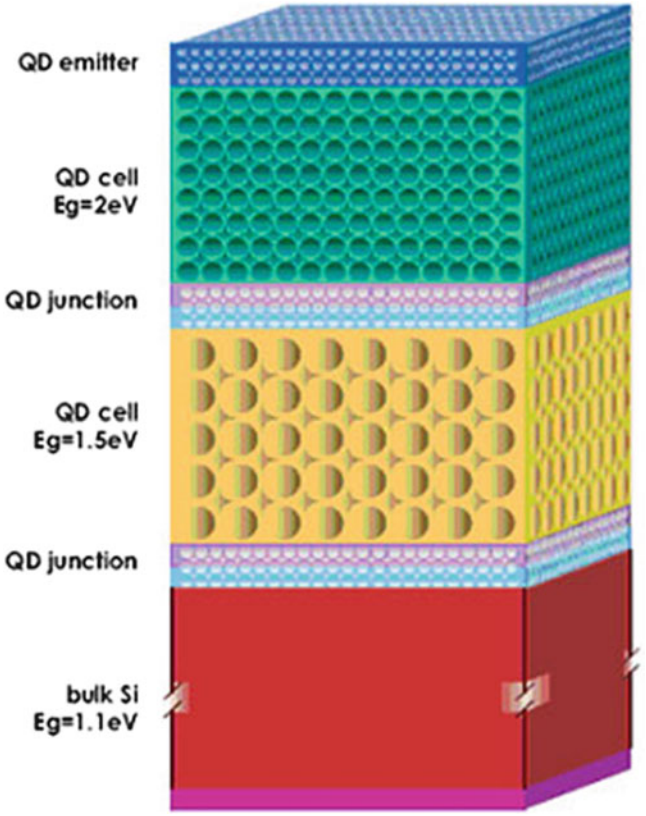

Fig. 3.10 Illustration of an all Si tandem solar cell structure based on different bandgap QD junctions (courtesy of the University of New South Wales)

momentum conservation, making the effect too small to be utilized for substantial efficiency enhancements. Nanostructured materials have been shown experimentally to increase the efficiency of carrier multiplication processes, with lower thresholds for carrier multiplication, and experimental demonstration of multiple exciton generation (MEG) in materials such as PbSe and PbS colloidal quantum dots [33, 34] with quantum efficiencies well in excess of 300%. The improved performance in nanocrystals over bulk systems is due to the relaxation of crystal momentum conservation in quantum dots, which in bulk systems together with energy conservation make the threshold for carrier multiplication roughly a factor of 1.5 higher than the bandgap. Due to quantum confinement, crystal momentum is no longer a good quantum number, and the threshold for carrier multiplication occurs at roughly multiples of the bandgap itself. Recent experimental evidence [35], as well as theoretical calculations [36], suggests indeed that the multiexcitation of several electron–hole pairs by single photons in quantum dot structures occurs at ultra-short time scales, without the necessity of impact

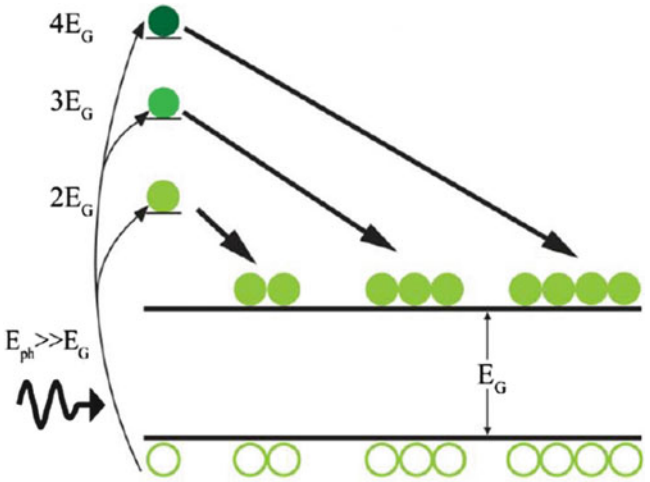

Fig. 3.11 Illustration of the multiexciton generation process for $M = 1, 2, 3$, and 4. The *lower panel* shows the calculated detailed balance efficiency as a function of bandgap with consideration of increasingly higher order multiplication factors

ionization. Overall, MEG generation has been shown in multiple materials, including PbSe, PbS, InAs [37], PbTe [38], Si [39], and CdSe [40].

While carrier multiplication has been shown in many materials, the key focus has been on lower band gap materials such as PbS and PbSe, partly because these materials show high quantum yields and partly because the theoretical optimum of a MEG solar cell is small at 0.76 eV. However, assuming more realistic conditions for carrier multiplication, the optimum band gap shifts to higher values, and Si becomes relatively ideal, as discussed below.

The increase in the efficiency of a solar cell due to MEG processes is calculated by using a quantum efficiency which is greater than unity for photon energies above the band gap. Ideally, a MEG solar cell generates two electron–hole pairs when the photon energy is between 2 and 3 times the band gap, 3 electron–hole pairs when the photon energy is between 3 and 4 times the band gap, etc. This is shown in Fig. 3.12 and in the equation below

$$Q(E) = \begin{cases} 0 & 0 < E < E_g \\ m & mE_g < E < (m+1)E_g \quad m = 1, 2, 3 \ldots \\ M & E \geq ME_g \end{cases}$$

where Q is the quantum efficiency (which is a function of energy), m is the number of electron–hole pairs generated by a photon, E_g is the threshold energy (which is ideally equal to the band gap energy), and M is the maximum number of electron–hole pairs generated.

The optimum band gap for a completely ideal MEG device is 0.76 eV [41], as shown in the detailed balance calculation of Fig. 3.13. However, the optimum low

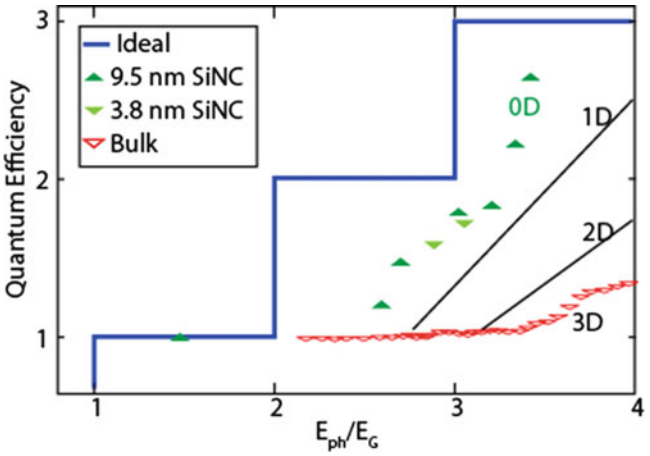

Fig. 3.12 Theoretical quantum efficiencies of a MEG solar cell, including the ideal quantum efficiency, the measured values for Si NC and bulk [40], and interpolated estimates for 1D and 2D

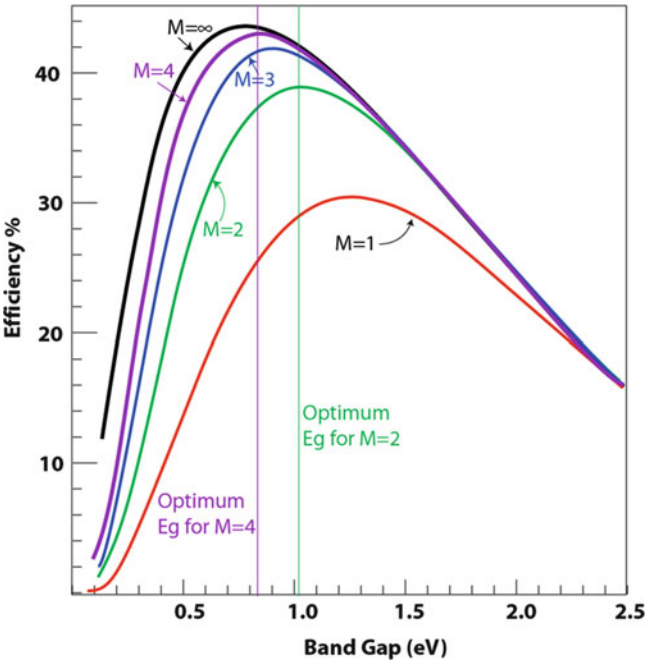

Fig. 3.13 Calculated detailed balance efficiency as a function of bandgap with consideration of increasingly higher order multiplication factors

band gap assumes the existence of multiple separate, noninteracting MEG generation processes, i.e., the band structure must be ideal for generating two excitons, as well as for three excitons, and so on, and also assumes that each of these MEG

processes does not interact. For example, all photons with energy 4 times the band gap (or the threshold energy) generate 4 excitons. However, in practice, some of these photons may generate 4 excitons, while others generate 2 or 3. Finally, the ideal calculations assume that the threshold energy for all the processes is equal to m times the band gap for each one.

Assuming that in practice it is difficult to generate more than several separate exciton generation pathways, the optimum band gap is increased, and the bandgap of silicon becomes relatively ideal. This is shown in Fig. 3.13, where the optimum band gap is 1.05 eV for $M = 2$. Overall, a Si MEG solar cell with $M = 2$ achieves 90% of the ideal maximum efficiency occurring at $M = \infty$ and optimum E_G. It is interesting to note that this is a higher fraction of the thermodynamic ideal that is achieved by materials used in three junction tandems, and assuming that 78% of the ideal material-imposed efficiency limit can be achieved in a well-optimized solar cell (true for both Si and III–V cells), the Si MEG solar cell realizes an efficiency of 30% while three-junction tandems at one sun have champion efficiencies of 32%.

An additional effect which needs to be included is the increase of the effective band gap due to the quantum confinement. The effective band gap in a Si nanocrystal can be increased and tuned according to the nanocrystal size. An empirical formula governing the effective band gap is given by $E(\text{eV}) = 1.16 + 11.8/d^2$ [42]. Si nanocrystals as large as 9.2 nm display among the highest MEG effects [40], and such large nanocrystals have relatively minor effect on the effective band gap (1.3 eV as opposed to 1.16 eV). Because the maximum efficiency is not sharply peaked as a function of band gap, because the nanocrystal size may be further increased, and because the effect of stress at the nanotip peaks serves to reduce the band gap, the effect of increasing effective band gap is not considered a strong factor.

MEG processes have strong experimental verification of the effect. While initial high values measured for the MEG processes are lower under re-measurements than those initially reported, values between 130% and 300% are confirmed. These lower values substantially reduce the efficiency potential of MEG processes. However, like many of such new processes, the theoretical understanding of the effects remains incomplete, and hence, in common with other approaches, the ability to design or predict optimum structures suffers.

An approach to developing the nanostructured Si surfaces with Si nanocrystals for MEG capture is to use nanosphere lithography (NSL) due to its combination of appropriate shape, the ability to incorporate surface QDs, and the realization of narrow tips. Other approaches, for example nanoimprint lithography, have also been used to make low reflection nanostructured surfaces [43]; nanosphere masking is better integrated into a conventional solar cell process. In addition, nanostructured surfaces can be made by photolithograph-based approaches [44], electron beam lithography [45], or direct growth of nanowires [46, 47], but such approach involves either considerable cost or complexity or are not as readily incorporated into a conventional solar cell.

The approach to realizing a nanostructured Si surface using nanosphere lithography is shown in Fig. 3.14. It is based on self-assembled monolayer (SAM) of QDs

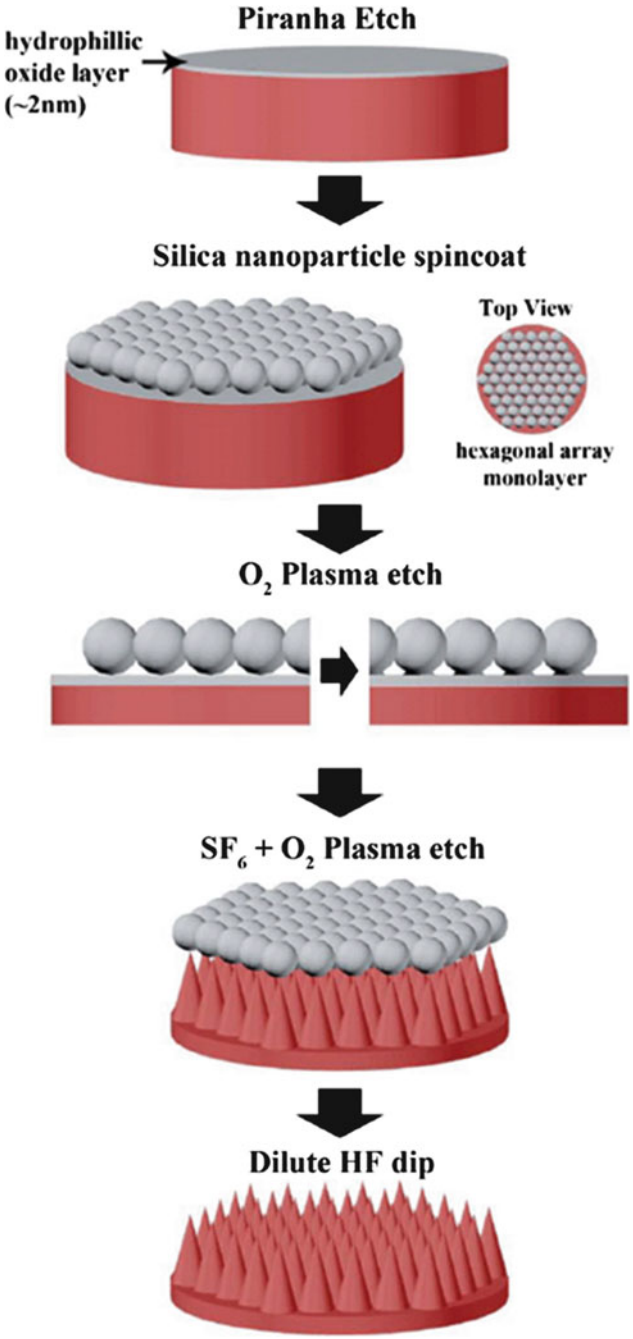

Fig. 3.14 Formation of nanotips of a Si surface

on the surface of a silicon solar cell. The initial demonstration of nanotips [48] uses SiO_2 nanospheres on the surfaces. These are chosen as they are available in good size uniformity, large area monolayers have been demonstrated on sapphire [49], there is good etch selectivity between SiO_2 and Si, and the SiO_2 nanospheres are stable in plasma etching. The spacing and height of the nanotips can be controlled by the size of the SiO_2 nanoparticles and the etching parameters.

The initial results demonstrate the feasibility of forming large area, defect free SiO_2 monolayers on a silicon surface, and the ability to use these spheres as an etch mask for the formation of nanotops. The surface preparation is a critical component of forming single SAMs. If the surface preparation and spincoat parameters are not optimized, then there are either areas with no nanoparticles or regions with multiple layers of nanoparticles, which interfere with the etching of the Si below. After some optimization of the surface properties and spin coat process, initial results demonstrate the ability to form large area, defect free regions with single SAM layers. Initial optimization allowed the realization of large, defect-free areas. For example, Fig. 3.15a shows a region several hundred micron on a side, with very low defects, while Fig. 3.15b shows a region with regions without SAM layers. Overall, the coverage over the entire 4 in. wafer is estimated at 60%. These results are achieved with no special modification of the surface beyond cleaning processes used in solar cell manufacturing or modification to the spin coat equipment, etc. Further, the cleaning processes did not use features such as continuous mixing, etc. which help insure the uniformity of cleans.

Initial results further show the suitability of the SAM layers as an etching mask. Figure 3.16 shows the cross-section of etched samples, with the QDs in place and with them removed following a dilute HF etch. Reactive Ion Etching (RIE) was used to etch the sample. The shape of the nanotips can be controlled by the size of the nanospheres and the etching time and properties. For example, for the given size of QDs, a shorter etching time gives a "blunter" tip due to the limited undercutting of the etching process. As the time in the RIE increases, the tips become narrower, forming 1D confinement as shown in Fig. 3.16c. The sample in Fig. 3.16c contained regions in which there were no Si QDs.

3.3.3 Intermediate Band Devices

Intermediate band solar cells, first suggested by Luque and Marti [12, 50], consist of an intermediate band between the conduction and valence band. This is shown conceptually in Fig. 3.17 for both quantum dots and quantum wells. Other realizations that have been proposed include impurity bands and bulk intermediate band materials that provide a narrow band within a larger bandgap directly from the crystal structure itself.

In order to give a thermodynamic increased efficiency, it is critical that the intermediate band be associated with its own quasi-Fermi level. If there is no separate quasi-Fermi level, then the efficiency of the overall concept collapses.

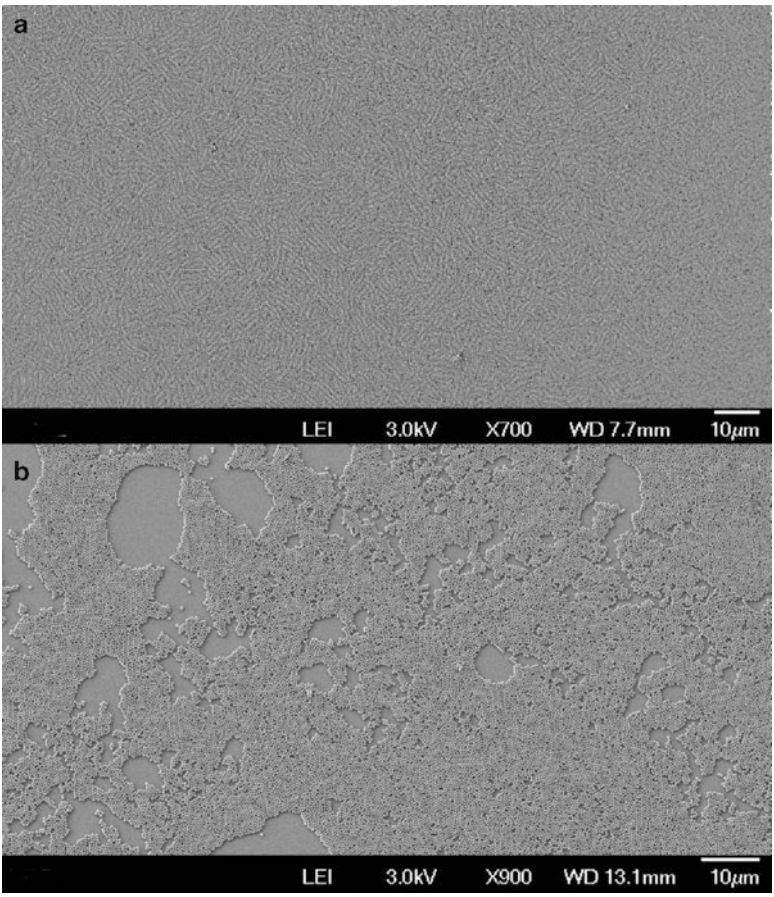

Fig. 3.15 (**a**) Large area, defect free region of single SAM coverage. (**b**) Coverage with several regions showing no SAM layers

Thus, the IB approach depends on achieving three sets of simultaneous absorption/radiative emission process (see Fig. 3.17), each having similar magnitudes, which in turn depends on realizing multiple quasi-Fermi levels. Assuming such ideal conditions, detailed balance can again be employed to calculate the maximum conversion efficiency as shown in Fig. 3.18. For any particular conduction band to intermediate band spacing, there is an optimum host bandgap giving maximum efficiency. Plotting the maximum efficiency versus the intermediate band energy, Luque and Marti were able to show that an optimum combination of host band gap (1.95 eV) and intermediate band energy (0.71 eV) leads to a maximum conversion efficiency of greater than 60% under concentration.

The three *individual* processes have a multitude of experimental evidence, with each being used in at least one commercial device [51–55]. However, the novelty and critical experimental parameter for the IB process is that the simultaneous

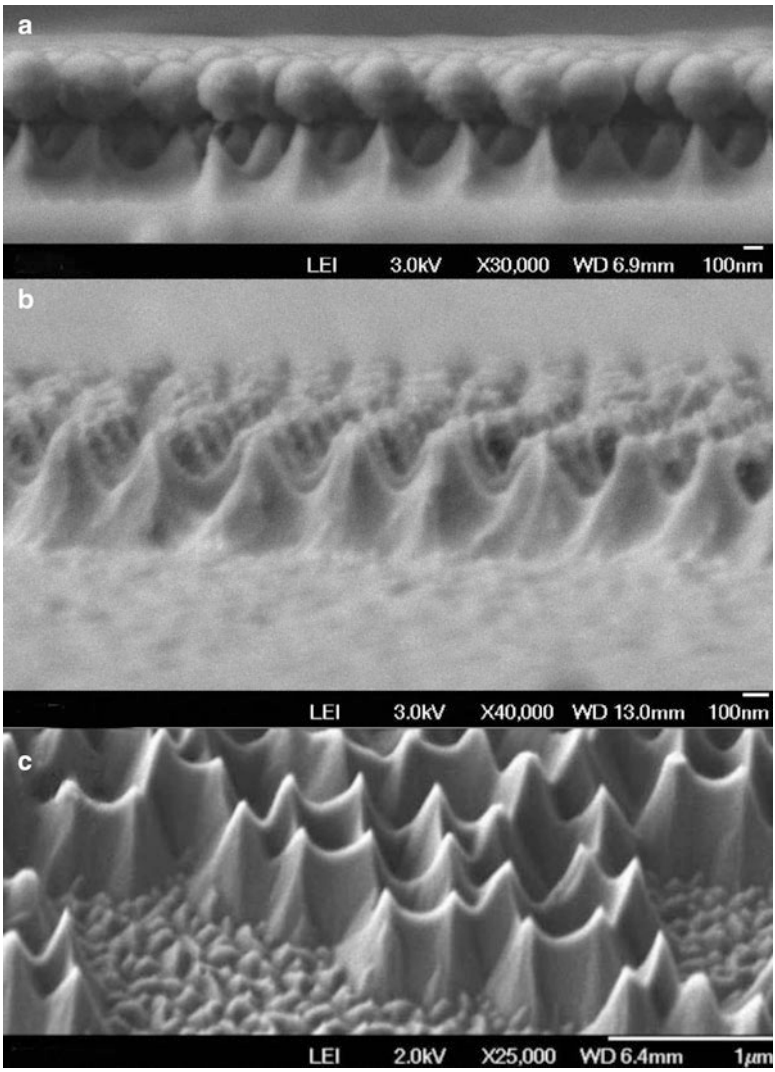

Fig. 3.16 Cross section of a single SAM layer on Si (**a**) with the QDs and (**b**) with the QDs removed; (**c**) nanotips with a very sharp tip, giving 1D confinement at the tip

processes giving rise to a separate quasi-Fermi level in the intermediate band. Recently, Marti et al. have reported important results [56] showing the ability to utilize two low energy photons to collect carriers at a higher energy, a necessary prerequisite for the IB effect. Furthermore, earlier results from Nelson et al. are explained [57] by a different Fermi level inside a QW than in the barrier. Despite these important results, the demonstration of an intermediate band effect consistent with a high efficiency process remains elusive. This is due to multiple,

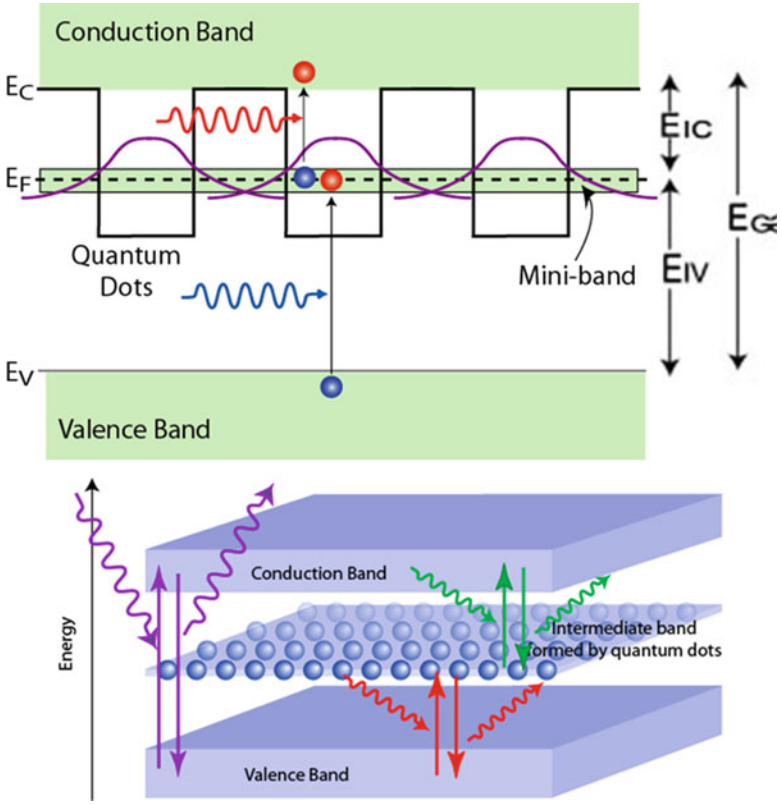

Fig. 3.17 Band diagram illustrating the realization of an intermediate band solar cell using quantum dots

interconnected reasons, relating to uncertainties about modeling and understanding the physical processes, measurement and experimental demonstration of multiple quasi-Fermi levels, identification of materials which display multiple quasi-Fermi level properties, and the design of devices based on measured properties.

In addition to the experimental demonstration of the effect, another critical issue in the intermediate band approaches is the search for optimum materials, which show appropriate band structure. While there are several bulk materials that show an intermediate band, most of the experimental work centers on using QD structures. QD structures are preferred to QW structures due to the low density of states between energy levels, which reduces scattering to lower energy levels. One limiting design rule is that the valence band offset should be small to reduce carrier recombination, increase hole collection in the contacts, and achieve a large open circuit voltage. One such material is GaAsSb/InAsP, which achieves a negligible valence band offset theoretically leads to close to ideal values for the host bandgap and intermediate band level, as shown in Fig. 3.19.

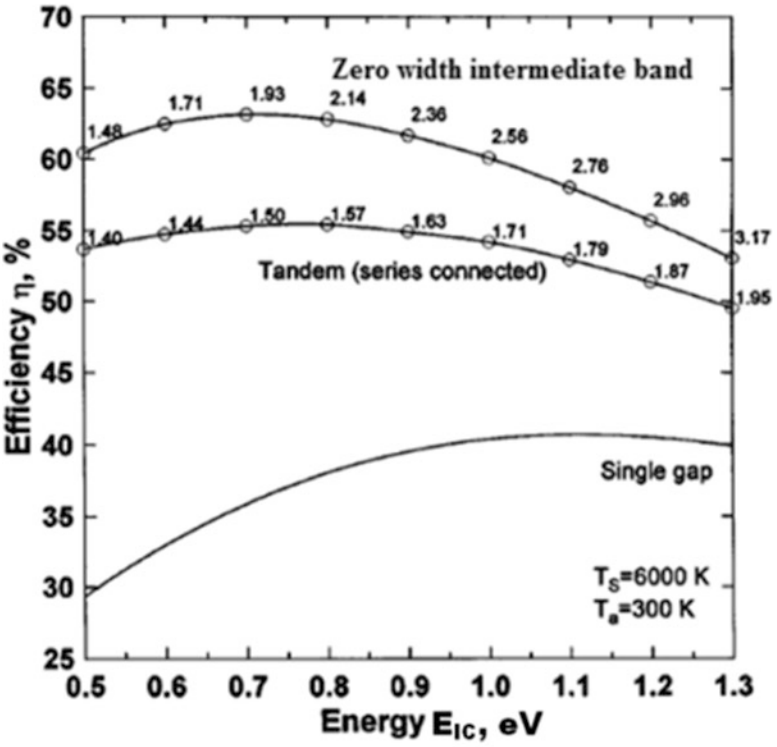

Fig. 3.18 Detailed balance efficiency as a function of the intermediate level energy (relative to the conduction band) for different host band gaps (from Luque et al. [12])

In addition to the composition and considerations of valence band offsets, the use of GaAsSb as a substrate material for the self-assembled growth of InAs quantum dots can lead to improved uniformity and reduced dot size [58]. Figure 3.20 shows the effect of different Sb mole fractions on the InAs dot density and size during epitaxial growth, showing reduction in size and increased coverage with increased Sb composition.

Another issue of importance for the operation of intermediate band solar cells in terms of the optimum quasi-Fermi level position is the appropriate doping of quantum dots, so that there is a balance of carriers excited optically from the intermediate band to the conduction band, and likewise from the valence band to the intermediate band [59]. Ideally this would correspond to half filled occupancy. Figure 3.21 shows a schematic of controllably filling the quantum dot states through a delta-doping layer of Si dopants, grown adjacent to the dots in the GaAs or GaAsSb barrier material. Time-integrated photoluminescence (PL) for samples with delta doping levels corresponding to 0, 2, 4, and 6 electrons per dot was measured as a function of both the excitation power and temperature. Typical

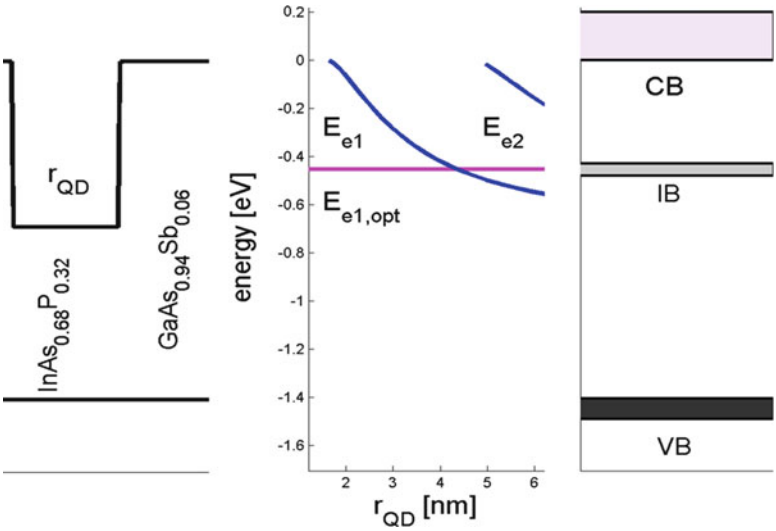

Fig. 3.19 Calculated conduction and valence band offsets for GaAsSb with InAsP quantum dots, and the corresponding energy levels for various quantum dot sizes

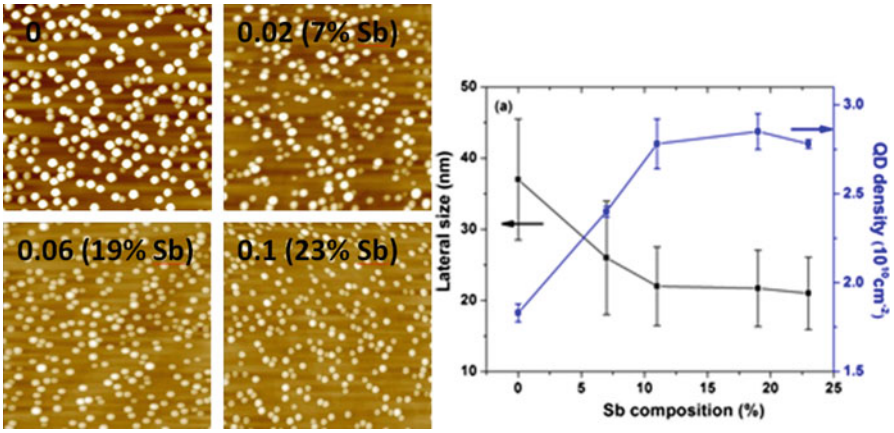

Fig. 3.20 AFM images of InAs QDs grown on the GaAs (5 ML)/$GaAs_{1-x}Sb_x$ (5 nm) buffer layers with various Sb compositions of 0 %, 7 %, and 23 %, respectively. *Right*: average lateral size (*left axis*), and dot density (*right axis*) of InAs QDs as a function of a Sb composition in the GaAsSb buffer layer [58]

spectra, shown in Fig. 3.22, illustrate the effect of doping on the dot PL spectra. For undoped samples, the dominant transition is from the ground state transition, whereas with increasing doping, the transition shifts to the first excited level within the quantum dot.

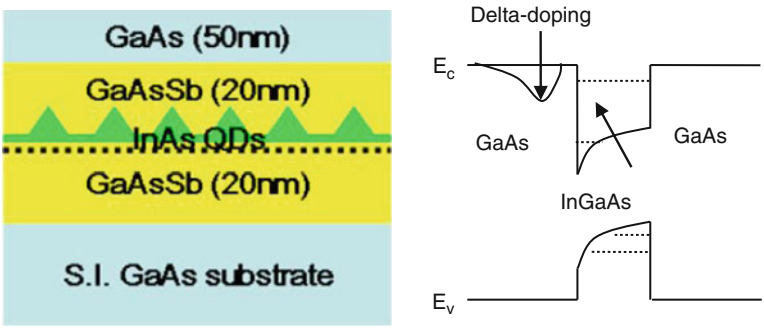

Fig. 3.21 Schematic of delta-doped InAs quantum dots in GaAsSb/GaAs for use as intermediate band states

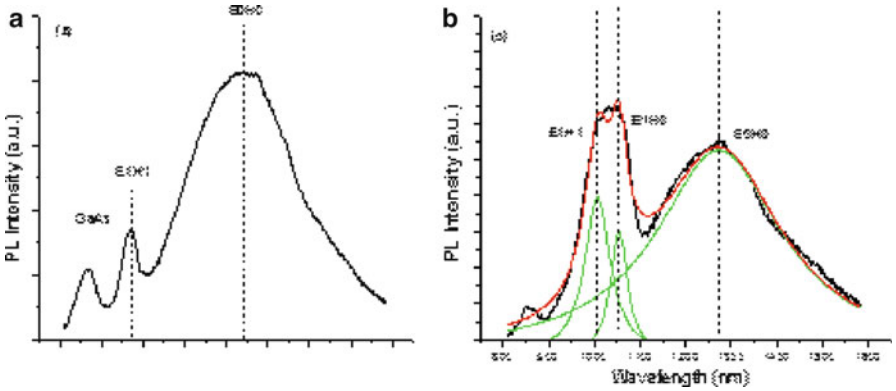

Fig. 3.22 Photoluminescence spectra from (**a**) undoped quantum dots and (**b**) Si-doped InAs QDs

3.3.4 Hot Carrier Solar Cells

Ross and Nozik proposed the concept of hot carrier solar cells [60] more than 25 years ago as a means to circumvent the limitations imposed by the Shockley–Queisser limit in terms of both the loss of excess kinetic energy and the loss of subbandgap photons. Figure 3.23 presents a schematic of the basic idea. The ideal absorber represents a material with a fundamental bandgap, $E_G \geq 0$, across which electron–hole pairs are excited by photons with energies greater than E_G. In the absorber, the relaxation of excess kinetic energy to the environment (i.e. the lattice) is suppressed, while the carriers themselves still interact strongly to establish a thermalized distribution, such that the electrons (and holes) are characterized by an effective temperature, T_H, much greater than the lattice

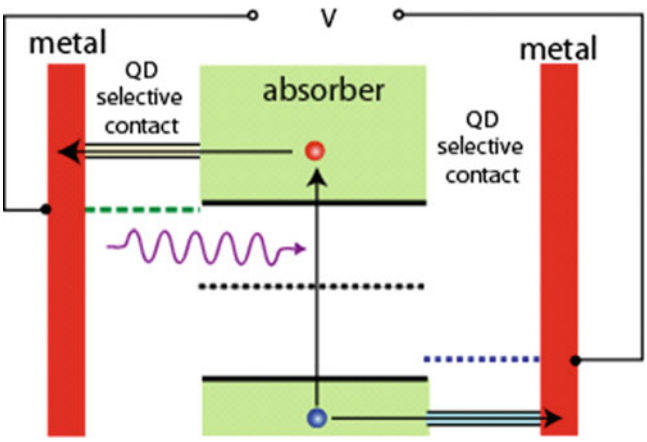

Fig. 3.23 Schematic of a hot-carrier solar cell consisting of an ideal absorber with energy selective contacts

temperature, T_L. This carrier temperature can be so large as to reverse the net chemical potential difference, μ_{ch}, between electrons and holes, and typically must be on the order of several thousand degrees for efficient operation.

Energy selective contacts are made to the absorber on the left and right, where the left contact extracts hot electrons in a narrow range of energies above the conduction band edge as shown, while the contact on the right extracts holes (injects electrons) at a specific energy range in the valence band. In this scheme, the electrons and hole are extracted from the system before they have time to relax their excess energy, hence utilizing the total energy of the photon. Under the assumption of no energy loss, the maximum efficiency occurs for vanishingly small bandgaps, hence capturing photons over the entire solar spectrum. In this limit, the theoretical detailed balance conversion efficiency approaches the maximum thermodynamic conversion efficiency of 85.4% [61]. More recently, Würfel and coworkers considered the effect of impact ionization and secondary carrier generation on the ultimate efficiency of this concept [62, 63].

There are many practical limitations to implementing this very ideal structure. One difficulty is realizing energy selective contacts. Würfel pointed out [63] that it is necessary to spatially separate the absorber material for the cold metallic contacts themselves, which may serve as an energy loss mechanism to the carriers in the absorber layer. There it was suggested that a large bandgap material such as GaN serve as a spacer or "membrane" separating the absorber from the contacts. Other proposals for energy selective contacts include using nanostructured resonant tunneling contacts from double barrier heterostructures, defects, or artificial quantum dots [64].

The main challenge in the technology is to realize an ideal absorber in which the excess kinetic energy of the photoexcited carriers is not lost to the environment.

There have been various proposals for reducing the carrier cooling rate. Due to the reduced dimensionality and therefore reduced density of final states in nanostructured systems, the energy loss rate due to phonons may be reduced, which has been observed experimentally [65]. In particular, in nanostructured systems such as quantum wells, quantum wires, or quantum dots, where intersubband spacing between levels is less than the optical phonon energy, then the optical emission rate may be suppressed due to the so-called phonon bottleneck effect, since there is no final states for the electron. However, even in such systems, the reduced phonon emission rate is still too fast for sufficient carrier heating, even under high solar concentration.

If, however, the energy is retained in the coupled electron–phonon system, then the energy would be recycled through hot phonon re-absorption. Nonequilibrium hot phonon effects during ultrafast photoexcitation have been well studied for many years. Time-resolved Raman scattering has been used, for example, to characterize the optical phonon decay after photoexcitation for a variety of III–V compound bulk and quantum well materials [66–69]. Ensemble Monte Carlo (EMC) simulation has previously been used to theoretically model ultrafast carrier relaxation and hot phonons effects in quantum well and bulk materials [70, 71], where hot phonons have been shown to significantly reduce the rate of carrier cooling compared to the bare energy loss rate.

Basically the main energy relaxation channel for electrons is through optical phonons, which lose energy through optical phonon emission in quanta of the optical phonon energy. However, due to the small group velocity of optical phonons, they do not leave the excitation volume; rather they must decay into acoustic phonons through a three phonon anharmonic scattering process, and it is the acoustic phonons which propagate energy away from the active region of the device. Hence electrons and holes may re-absorb the excess phonons, and so the excess kinetic energy of the photoexcited EHPs remains in the system until the optical phonons decay to acoustic modes. It has recently been argued by the UNSW group that nonequilibrium "hot" phonons may play a critical role in reducing carrier energy loss and maintaining energy within the absorber [72]. Typical optical phonon decay times range from 1 to 10 ps, much longer than the electron optical phonon emission rate (which is subpicosecond in scale). Engineering materials as absorbers with long phonon decays, particularly nanoengineered structures, are currently being investigated [72].

Figure 3.24 shows the simulated effect of phonon lifetime on carrier relaxation using EMC simulation, similar to earlier work on this topic [70, 73]. Here a 2 eV laser pulse exciting a 10 nm GaAs/AlAs QW is simulated, which peaks at 1 ps into the simulation, and is 200 fs wide. Optical absorption is modeled by creating electron–hole pairs corresponding to photons with a given frequency and momentum. Figure 3.24 plots the carrier temperature as a function of time for various assumed phonon lifetimes ranging from 0 (i.e. no hot phonons) to 100 ps. Additionally, one curve is included in which electron–hole scattering is suppressed.

As can be seen in the simulated results of Fig. 3.24, without hot phonons, the electrons cool rapidly and reach the lattice temperature within 5–10 ps. In contrast,

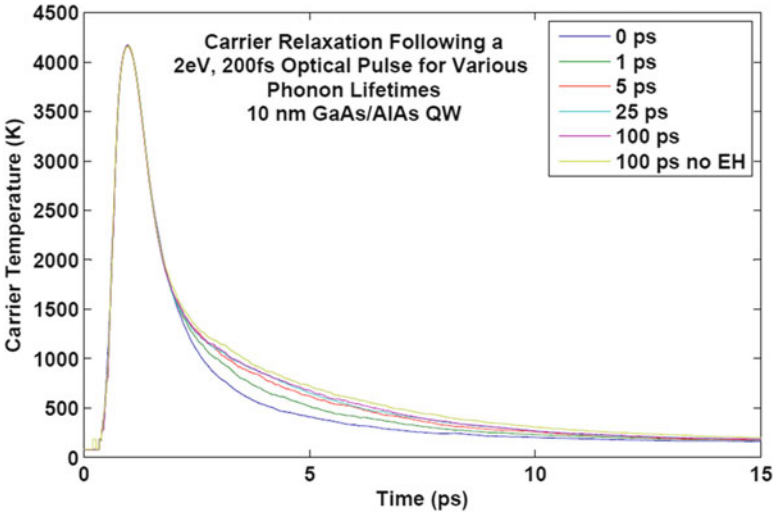

Fig. 3.24 Simulated electron temperature versus time for various assumed phonon lifetimes in a 10 nm GaAs/AlAs QW following a 2 eV, 200 fs wide optical pulse. The injected carrier density is $5 \times 10^{11}/\text{cm}^2$ in all cases. The lattice temperature is 5 K (S. M. Goodnick et al. [73])

with hot phonons, after the initial pulse, when a nonequilibrium distribution of hot phonons establishes itself, the decay slows and becomes nonexponential. However, for large phonon lifetimes, the decay rate does not change significantly, indicating that other channels are present for energy relaxation in the system. To check one of these, we suppress electron–hole scattering, so that energy is not taken from the electron system and transferred to the hole system, where nonpolar phonon scatter removes energy. As can be seen, the effect is not very large, and there is only a small decrease in the net relaxation rate for a phonon lifetime of 100 ps.

If the energy in the absorber is retained in the coupled electron/hole–phonon system, and only decays as the optical phonon decay, then one can look at the excess carrier energy in steady state under solar irradiation using energy balance

$$\left.\frac{\partial E}{\partial t}\right|_{\text{phonons}} + \left.\frac{\partial E}{\partial t}\right|_{\text{extr}} + \left.\frac{\partial E}{\partial t}\right|_{\text{rec}} = \left.\frac{\partial E}{\partial t}\right|_{\text{optical}} \tag{3.2}$$

The term on the right represents the average excess kinetic energy provided to the coupled electron–hole system from photoexcited carriers, whereas the first term on the left represents the energy loss rate due to optical phonons, the second term is the energy loss from the absorber due to hot carriers extracted through energy selective contacts, and the third term is the energy loss due to recombination.

The average excess energy from photons above the absorber bandgap available for carrier heating may be calculated from the appropriate solar spectrum. Figure 3.25a shows the average excess kinetic energy versus bandgap calculated from an average of the black body AM0 distribution.

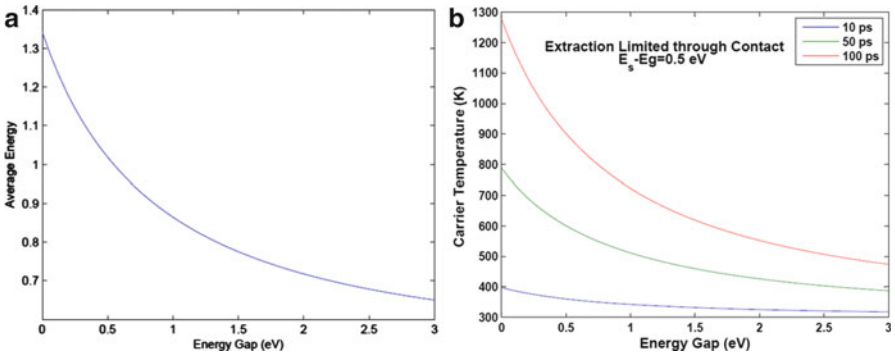

Fig. 3.25 (**a**) Average excess kinetic energy, E_{exc}, available for carrier heating as a function of bandgap based on the blackbody solar spectrum. (**b**) Calculated hot carrier temperature, T_H, for various phonon lifetimes assuming a 1 ns extraction time (from S. Goodnick et al. [73])

Using the result of Fig. 3.25a for E_{exc}, the calculated carrier temperature, T_H, as a function of bandgap for several different phonon lifetimes is plotted in Fig. 3.25b. As can be seen, for significant carrier heating to occur, long optical phonon lifetimes are required with a small gap absorber, several 10s of picoseconds, which is longer than the values measured in bulk materials, which is typically in the range from 1 to 10 ps.

The main conclusion of this analysis is that for sufficiently long energy relaxation times, hot carrier temperatures sufficient for hot carrier extraction through selective contacts are expected, leading to potentially high energy conversion efficiency. The realization of such long energy relaxation times is of course challenging and will inevitably require a combination of phonon engineering and nanostructured absorbers to suppress phonon emission.

3.3.5 Hybrid Concepts

In the previous sections, we have briefly discussed some of the advanced concept solar cell structures, and how nanotechnology can benefit the realization of these concepts. An innovation on advanced concept devices is to consider hybrids of several concepts, which allow one to exceed to potential and overcome material-specific limitations of any particular technology. Figure 3.26 shows the detailed balance calculation of the 1 sun conversion efficiency of a hot carrier solar cell versus the limits for intermediate band and multiple exciton generation solar cells, which has the potential for over 50% conversion at 1 sun, and closer to the thermodynamic limit of 86.5% at maximum concentration. Also shown is the calculated efficiency for a hybrid converter, which combines one or more concepts such as hot carrier and intermediate band [74]. As shown, the potential for such hybrid converters is greater than that of single concept approaches.

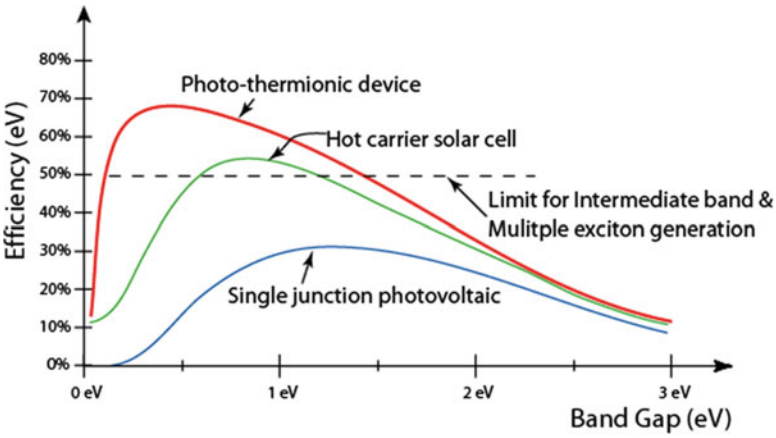

Fig. 3.26 Comparison of the detailed balance calculation of the 1 sun efficiency for a hot carrier solar cell, and a hybrid thermo-photonic device, illustrating the improvement with respect to the single gap limit

3.4 Summary

To date, many of the principles of new concept solar cells have been demonstrated as discussed earlier. However, the measured improvements in solar cell efficiency with the inclusion of nanostructures have been limited due to a variety of issues. One is the inherent problem of surfaces and interfaces in solar cells, and their passivation. Surface recombination is detrimental in terms of both reduced photocurrent affecting short circuit current and in an increase in dark current, which reduces the open circuit voltage and hence maximum power of a solar cell. Due to the high surface-to-volume ratio of nanostructured materials, they are more sensitive to surface effects than bulk materials. Therefore, effective approaches to passivate surfaces in nanostructures are necessary to incorporate them as components in the active regions of the device such as in the approaches discussed earlier. Another issue is the lack of optimization of the material structures in terms of their electronic structure and associated optical properties for the intended applications. Considerable work remains to determine the optimum nanomaterial composition and structure to realize the potential of new concept solar cells. With improvements in nanostructure growth and synthesis, it is expected that these issues will be addressed, and that benefits realized in both improved efficiency and reduction in manufacturing costs in maintaining the growth curve of photovoltaics to the TW scale.

References

1. R.E. Smalley, Future global energy prosperity: The terawatt challenge. MRS Bull. **30**, 412–417 (2005)
2. N.A. Lewis, Powering the Planet. DOE Program Review (2005)

3. W. Shockley, H.J. Queisser, Detailed balance limit of efficiency of p-n junction solar cells. J. Appl. Phys. **32**, 510–519 (1961)
4. Solar Junction tips 43.5% efficient CPV cell, preps 250 MW capacity ramp. Photovoltaics World, Photovoltaics-CPV, Issue 2, March 2011
5. R.T. Ross, A.J. Nozik, Efficiency of hot-carrier solar energy converters. J. Appl. Phys. **53**, 3813–3818 (1982)
6. K.W.J. Barnham, G. Duggan, A new approach to multi bandgap solar cells. J. Appl. Phys. **67**, 3490 (1990)
7. S. Kolodinski, J.H. Werner, T. Wittchen, H.J. Queisser, Quantum efficiencies exceeding unity due to impact ionization in silicon solar cells. Appl. Phys. Lett. **63**, 2405 (1993)
8. M.A. Green, *Third Generation Photovoltaics: Advanced Energy Conversion* (Springer, Berlin, 2003)
9. S. Kolodinski, J.H. Werner, T. Wittchen, H.J. Queisser, Quantum efficiencies exceeding unity due to impact ionization in silicon solar cells. Appl. Phys. Lett. **63**, 2405 (1993)
10. R. Schaller, V. Klimov, High efficiency carrier multiplication in pbse nanocrystals: Implications for solar energy conversion. Phys. Rev. Lett. **92**, 186601 (2004)
11. H. Cotal, C. Fetzer, J. Boisvert, G. Kinsey, R. King, P. Hebert, H. Yoon, N. Karam, III-V multijunction solar cells for concentrating photovoltaics. Energy Environ. Sci. **2**, 174–192 (2009)
12. A. Luque, A. Martí, Phys. Rev. Lett. **78**, 5014 (1997)
13. R.T. Ross, A.J. Nozik, Efficiency of hot-carrier solar energy converters. J. Appl. Phys **53**, 3813 (1982)
14. P. Würfel, Solar energy conversion with hot electrons from impact ionization. Sol. Energy Mater. Sol. Cells **46**, 43 (1997)
15. P. Würfel, A.S. Brown, T.E. Humphrey, M.A. Green, Particle conservation in the hot-carrier solar cell. Prog. Photovolt. Res. Appl. **13**, 277 (2005)
16. A.Y. Cho, J.R. Arthur, Molecular beam epitaxy. Prog. Solid State Chem. **10**, 157–191 (1975)
17. W. Lu, C.M. Lieber, Semiconductor nanowires. J. Phys. D Appl. Phys. **39**, R387 (2006)
18. L. Samuelson, Self-forming nanoscale devices. Mater. Today **6**, 22–31 (2003)
19. M.T. Björk, B.J. Ohlsson, T. Sass, A.I. Persson, C. Thelander, M.H. Magnusson, K. Deppert, L.R. Wallenberg, L. Samuelson, One-dimensional steeplechase for electrons realized. Nano Lett. **2**, 87–89 (2002)
20. M.T. Björk, B.J. Ohlsson, C. Thelander, A.I. Persson, K. Deppert, L.R. Wallenberg, L. Samuelson, Nanowire resonant tunneling diodes. Appl. Phys. Lett. **81**, 4458–4460 (2002)
21. C. Thelander, T. Martensson, M.T. Björk, B.J. Ohlsson, M.W. Larsson, L.R. Wallenberg, L. Samuelson, Single-electron transistors in heterostructure nanowires. Appl. Phys. Lett. **83**, 2052–2054 (2003)
22. A. Fuhrer, C. Fasth, L. Samuelson, Single electron pumping in InAs nanowire double quantum dots. Appl. Phys. Lett. **91** (2007). doi:10.1063/1.2767197
23. A. Fuhrer, L.E. Froberg, J.N. Pedersen, M.W. Larsson, A. Wacker, M.E. Pistol, L. Samuelson, Few electron double quantum dots in InAs/InP nanowire heterostructures. Nano Lett. **7**, 243–246 (2007)
24. M.T. Björk, A. Fuhrer, A.E. Hansen, M.W. Larsson, L.E. Jensen, L. Samuelson, Tunable effective g factor in InAs nanowire quantum dots. Phys. Rev. B **72**, 201307 (2005)
25. A.P. Alivisatos, Perspectives on the physical chemistry of semiconductor nanocrystals. J. Phys. Chem. **100**, 13226–13239 (1996)
26. D. Bimberg, M. Grundmann, N.N. Ledentsov, *Quantum Dot Heterostructures* (Wiley, Chichester, UK, 1999)
27. H.W. Kroto, J.R. Heath, S.C. O'Brien, R.F. Curl, R.E. Smalley, C60: Buckminsterfullerene. Nature **318**, 162–163 (1985)
28. M.S. Dresselhaus, G. Dresselhaus, P.C. Eklund, *Science of Fullerenes and Carbon Nanotubes* (Academic Press, New York, 1996)

29. T. Dürkop, S.A. Getty, E. Cobas, M.S. Fuhrer, Extraordinary mobility in semiconducting carbon nanotubes. Nano Lett. **4**, 35–39 (2003)
30. A. Javey, J. Guo, Q. Wang, M. Lundstrom, H. Dai, Ballistic carbon nanotube field-effect transistors. Nature **424**, 654–657 (2003)
31. P.L. McEuen, M.S. Fuhrer, P. Hongkun, Single-walled carbon nanotube electronics. IEEE Trans. Nanotechnol. **1**, 78–85 (2002)
32. S. Kolodinski, J.H. Werner, T. Wittchen, H.J. Queisser, Quantum efficiencies exceeding unity due to impact ionization in silicon solar cells. Appl. Phys. Lett. **63**(17), 2405–2407 (1993)
33. R.D. Schaller, V.I. Klimov, High efficiency carrier multiplication in PbSe nanocrystals: implications for solar energy conversion. Phys. Rev. Lett. **92**(18), 186601 (2004)
34. R.J. Ellingson, M.C. Beard, J.C. Johnson, P. Yu, O.I. Micic, A.J. Nozik, A. Shabaev, A.L. Efros, Highly efficient multiple exciton generation in colloidal PbSe and PbS quantum dots. Nano Lett. **5**(5), 865–871 (2005)
35. A.J. Nozick, Exciton multiplication and relaxation dynamics in quantum dots: Applications to ultrahigh-efficiency solar photon conversion. Inorg. Chem. **44**, 6893 (2005)
36. A. Shabaev, A.L. Efros, A.J. Nozik, Multiexciton generation by a single photon in nanocrystals. Nano Lett. **6**, 8 (2006)
37. R.D. Schaller, J.M. Pietryga, V.I. Klimov, Carrier multiplication in InAs nanocrystal quantum dots with an onset defined by the energy conservation limit. Nano Lett. **7**(11), 3469–76 (2007)
38. J.E. Murphy, M.C. Beard, A.G. Norman, S. Phillip, J.C. Johnson, S.P. Ahrenkiel, O.I. Micic, P. Yu, R.J. Ellingson, A.J. Nozik, PbTe colloidal nanocrystals: Synthesis, characterization, and multiple exciton generation. J. Am. Chem. Soc. **128**(10), 3241–3247 (2006)
39. J.H. Werner, S. Kolodinski, H.J. Queisser, Novel optimization principles and efficiency limits for semiconductor solar cells. Phys. Rev. Lett. **72**(24), 3851–4 (1994)
40. M.C. Beard, K.P. Knutsen, P. Yu, J.M. Luther, Q. Song, W.K. Metzger, R.J. Ellingson, A.J. Nozik, Multiple exciton generation in colloidal silicon nanocrystals. Nano Lett. **7**(8), 2506–2512 (2007)
41. A. de Vos, B. Desoete, On the ideal performance of solar cells with larger-than-unity quantum efficiency. Sol. Energy Mater. Sol. Cells **51**(3), 413–424 (1998)
42. T.-Y. Kim, N.-M. Park, K.-H. Kim, Y.-W. Ok, T.-Y. Seong, C.-J. Choi, G.Y. Sung, Quantum confinement effect of silicon nanocrystals in situ grown in silicon nitride films. Mater. Res. Soc. Symp. Proc. **817**, L4.3 (2004)
43. Q. Chen, G. Hubbard, P.A. Shields, C. Liu, D.W.E. Allsopp, W.N. Wang, S. Abbott, Broadband moth-eye antireflection coatings fabricated by low-cost nanoimprinting. Appl. Phys. Lett. **94**(26), 263118 (2009)
44. Y.M. Song, S.Y. Bae, J.S. Yu, Y.T. Lee, Closely packed and aspect-ratio-controlled antireflection subwavelength gratings on GaAs using a lenslike shape transfer. Opt. Lett. **34**(11), 1702–4 (2009)
45. S.A. Boden, D.M. Bagnall, Tunable reflection minima of nanostructured antireflective surfaces. Appl. Phys. Lett. **93**(13), 133108 (2008)
46. N. Wang, Y. Cai, R.Q. Zhang, Growth of nanowires. Mater. Sci. Eng. R Rep. **60**(1), 1–51 (2008)
47. M.D. Kelzenberg, D.B. Turner-Evans, B.M. Kayes, M.A. Filler, M.C. Putnam, N.S. Lewis, H. A. Atwater, Photovoltaic measurements in single-nanowire silicon solar cells. Nano Lett. **8**(2), 710–14 (2008)
48. Sean's thesis
49. T. Ogi, K. Okuyama, L.B. Modesto-Lopez, F. Iskandar, Fabrication of a large area monolayer of silica particles on a sapphire substrate by a spin coating method. Colloids Surf. A Physicochem. Eng. Asp. **297**(1), 71–78 (2007)
50. A. Luque, A. Martí, The intermediate band solar cell: Progress toward the realization of an attractive concept. Adv. Mater. **22**, 160–174 (2010)

51. Y. Yao, W.O. Charles, T. Tsai, G. Wysocki, J. Chen, C.F. Gmachl, Broadband quantum cascade laser gain medium based on a "continuum-to-bound" active region design. Appl. Phys. Lett. **96**(21), 211106 (2010)
52. P. Bhattacharya, A.D. Stiff-Roberts, S. Krishna, S. Kennerly, Quantum dot infrared detectors and sources. Int. J. High Speed Electron. Syst. **12**(4), 969–94 (2002)
53. H.F. MacMillan, H.C. Hamaker, N.R. Kaminar, M.S. Kuryla, M.L. Ristow, D.D. Liu, G.F. Virshup, J.M. Gee, 28% Efficient GaAs concentrator solar cells. IEEE Photovoltaic Specialists Conference, pp. 462–8 (1988)
54. C.G. Bailey, D.V. Forbes, R.P. Raffaelle, S.M. Hubbard, Near 1 V open circuit voltage InAs/GaAs quantum dot solar cells. Appl. Phys. Lett. **98**, 163105 (2011)
55. S. Sauvage, P. Boucaud, F.H. Julien, J.-M. Gérard, V. Thierry-Mieg, Intraband absorption in n-doped InAs/GaAs quantum dots. Appl. Phys. Lett. **71**, 2785 (1997)
56. A. Martí, E. Antolín, C.R. Stanley, C.D. Farmer, N. López, P. Díaz, E. Cánovas, P.G. Linares, A. Luque, Production of photocurrent due to intermediate-to-conduction-band transitions: A demonstration of a key operating principle of the intermediate-band solar cell. Phys. Rev. Lett. **97**, 247701 (2006)
57. J. Nelson, J. Barnes, N. Ekins-Daukes, B. Kluftinger, E. Tsui, K. Barnham, C. Tom Foxon, T. Cheng, J. Roberts, Observation of suppressed radiative recombination in single quantum well p- i- n photodiodes. J. Appl. Phys. **82**, 6240 (1997)
58. K.-Y. Ban, S.P. Bremner, G. Liu, S.N. Dahal, P.C. Dippo, A.G. Norman, C.B. Honsberg, Use of a GaAsSb buffer layer for the formation of small, uniform, and dense InAs quantum dots. Appl. Phys. Lett. **96**, 183101 (2010)
59. K.-Y. Ban, S.P. Bremner, G. Liu, S.N. Dahal, P.C. Dippo, A.G. Norman, C.B. Honsberg, Controllability of the subband occupation of InAs quantum dots on a delta-doped GaAsSb barrier. J. Appl. Phys. **109**, 014312 (2011)
60. R.T. Ross, A.J. Nozik, Efficiency of hot-carrier solar energy converters. J. Appl. Phys. **53**, 3813–3818 (1982)
61. P.T. Landsberg, G. Tonge, Thermodynamic energy conversion efficiencies. J. Appl. Phys. **5**(1), R1 (1980)
62. P. Würfel, Solar energy conversion with hot electrons from impact ionization. Sol. Energy Mater. Sol. Cells **46**, 43–52 (1997)
63. P. Würfel, A.S. Brown, T.E. Humphrey, M.A. Green, Particle conservation in the hot-carrier solar cell. Prog. Photovolt. Res. Appl. **13**, 277 (2005)
64. G. Conibeer, M.A. Green, R. Corkish, Y. Cho, E. Chob, C. Jiang, T. Fangsuwannarak, E. Pink, Y. Huang, T. Puzzer, T. Trupke, B. Richards, A. Shalav, K. Lind, Silicon nanostructures for third generation photovoltaic solar cells. Thin Solid Films **511–512**, 654 (2006)
65. W.S. Pelouch, R.J. Ellingson, P.E. Powers, C.L. Tang, D.M. Szmyd, A.J. Nozik, Comparison of hot-carrier relaxation in quantum wells and bulk GaAs at high carrier densities. Phys. Rev. B **45**, 1450–1453 (1992)
66. K.S. Tsen, K.R. Wald, T. Ruf, P.Y. Yu, H. Morkoc, Electron optical phonon interactions in ultrathin GaAs AlAs multiple quantum well structures. Phys. Rev. Lett. **67**, 2557–2560 (1991)
67. K.T. Tsen, R.P. Joshi, D.K. Ferry, A. Botcharev, B. Sverdlov, A. Salvador, H. Morkoc, Non-equlibrium electron distributions and phonon dynamics in wurtzite GaN. Appl. Phys. Lett. **68**, 2990–2992 (1996)
68. K.T. Tsen, J.G. Kiang, D.K. Ferry, H. Morkoc, Subpicosecond time-resolved Raman studies of LO phonons in GaN: Dependence on photoexcited carrier density. Appl. Phys. Lett. **89**, 112111 (2006)
69. K.T. Tsen, J.G. Kiang, D.K. Ferry, H. Lu, W.J. Schaff, H.-W. Lin, S. Gwo, Direct measurements of the lifetimes of longitudinal optical phonon modes and their dynamics in InN. Appl. Phys. Lett. **90**, 152107-1-3 (2007)
70. S.M. Goodnick, P. Lugli, Hot carrier relaxation in quasi-2D systems, in *Hot Carriers in Semiconductor Microstructures: Physics and Applications*, ed. by J. Shah (Academic, New York, 1992), pp. 191–234

71. M. Dür, S.M. Goodnick, P. Lugli, Monte Carlo simulation of intersubband relaxation in wide, uniformly doped GaAs/AlxGa1-xAs quantum wells. Phys. Rev. **B54**, 17794 (1996)
72. G. Conibeer, R. Patterson, L. Huang, J.-F. Guillemoles, D. König, S. Shrestha, M.A. Green, Modelling of hot carrier solar cell absorbers. Sol. Energy Mater. Sol. Cells **94**, 1516–1521 (2010)
73. S.M. Goodnick, C. Honsberg, Modeling carrier relaxation in hot carrier solar cells. Proc. SPIE. **8256**, 82560W (2012). doi:10.1117/12.910858
74. C.B. Honsberg, J. Lee, A. Bailey, S. Dahal, Hybrid advanced concept solar cells. Proceedings of the 37th IEEE Photovoltaics Specialists Conference, Seattle, WA, 2011